Available online at www.sciencedirect.com
SCIENCE DIRECT®
Journal of Theoretical Biology 232 (2005) 467–490
Journal of Theoretical Biology
www.elsevier.com/locate/yjtbi

The dynamics of single-substrate continuous cultures: The role of ribosomes

Shakti Gupta[a], S.S. Pilyugin[b], Atul Narang[a,*]

[a]Department of Chemical Engineering, University of Florida, Gainesville, FL 32611-6005, USA
[b]Department of Mathematics, University of Florida, Gainesville, FL 32611-8105, USA

Received 18 March 2004; received in revised form 2 August 2004; accepted 31 August 2004

Abstract

When a chemostat is perturbed from its steady state, it displays complex dynamics. For instance, if the identity of the growth-limiting substrate is switched abruptly, the substrate concentration and cell density undergo a pronounced excursion from the steady state that can last several days. These dynamics occur because certain physiological variables respond slowly. In the literature, several physiological variables have been postulated as potential sources of the slow response. These include transport enzymes, biosynthetic enzymes, and ribosomes. We have been addressing this problem by systematically exploring the role of these variables. In previous work Shoemaker et al. (J. Theor. Biol., 222 (2003) 307–322), we studied the role of transport enzymes, and we showed that transients starting from low transport enzyme levels could be quantitatively captured by a model taking due account of transport enzyme synthesis. However, there is some experimental data indicating that slow responses occur even if the initial enzyme levels are high. Here, we analyse this data to show that in these cases, the sluggish response is most probably due to slow adjustment of the ribosome levels. To test this hypothesis, we extend our previous model by accounting for the evolution of both the transport enzyme and the ribosomes. Based on a kinetic analysis of the data in the literature, we assume that the specific protein synthesis rate is proportional to the ribosome level, and the specific ribosome synthesis rate is autocatalytic. Simulations of the model show remarkable agreement with experimentally observed steady states and the transients. Specifically, the model predictions are in good agreement with (1) the steady-state profiles of the cell density, substrate concentration, RNA, proteins, and transport enzymes, (2) the instantaneous specific substrate uptake, growth, and respiration rates in response to a continuous-to-batch shift, and (3) the transient profiles of the cell density, substrate concentration, and RNA in response to feed switches and dilution rate shifts. Time-scale analysis of the model reveals that every transient response is a combination of two fundamental (and simpler) dynamics, namely, substrate-sufficient batch dynamics and cell-sufficient fed-batch dynamics. We obtain further insight into the transient response by analysing the equations describing these fundamental dynamics. The analysis reveals that in feed switches or dilution rate shift-ups, the transport enzyme reaches a maximum before RNA achieves its maximum, and in dilution rate shift-downs the cell density reaches a maximum before RNA achieves a minimum.

Keywords: Microbial growth; Structured model; RNA; Transients

1. Introduction

The chemostat is a convenient laboratory approximation to natural water bodies. Consequently, microbial growth in a chemostat is of fundamental interest in microbial ecology (Egli, 1995). In natural water bodies, many bacterial species grow simultaneously on mixtures of several growth-limiting substrates. However, these complex systems cannot be fully understood until questions concerning the growth of only one species on a single growth-limiting substrate have been resolved.

*Corresponding author. Tel.: +1 352 392 0028; fax: +1 352 392 9513.
E-mail address: anarang@che.ufl.edu (A. Narang).

0022-5193/$ - see front matter © 2004 Elsevier Ltd. All rights reserved.
doi:10.1016/j.jtbi.2004.08.025

Chemostat dynamics are also important from an engineering standpoint (Nielsen and Villadsen, 1992). Industrial bioreactors are prone to abrupt changes in the flow rate and feed concentrations. The transient response to these perturbations frequently involves massive loss of cells from the reactor and overshoots of the substrate concentration (see, for instance, Figs. 1 and 2). These dynamics can cause regulatory violations in wastewater treatment plants and product deterioration in industrial fermenters. A mathematical theory of chemostat dynamics would facilitate the development of rational operating protocols and model-based control strategies (Ramkrishna, 2003).

The cell loss and substrate overshoot occur because of slow physiological adaptation. Although the environment changes rapidly, the specific growth and substrate uptake rates of the cells respond slowly (Fig. 2c). Since these rates are in turn determined by some intracellular components, the question arises: Which intracellular components are responsible for the slow response of the specific growth and substrate uptake rates?

We are addressing this question by systematically investigating the role of potential candidates. In recent work, we studied the role of *peripheral enzymes*, i.e., the enzymes that catalyse the transport and peripheral catabolism of substrates (Shoemaker et al., 2003). This study was motivated by the dynamics of *substrate switches*. Fig. 1 shows an example of such an experiment. When the growth-limiting carbon source of a *C. heintzii* culture is switched from glucose to nitrilotriacetic acid (NTA), there is almost no substrate uptake, and hence, no growth for ~ 30 h (see Figs. 1a,b). We argued that this is because synthesis of the peripheral enzymes for NTA is inducible, and hence, autocatalytic. Since the cells have not seen NTA until the substrate is switched, the initial level of the peripheral enzymes for NTA is vanishingly small (Fig. 1c). Because inducible enzyme synthesis is autocatalytic, it takes several hours to build sufficiently high levels of these enzymes. We showed that a model taking due account of inducible enzymes and their autocatalytic synthesis captured these dynamics quantitatively (Shoemaker et al., 2003).

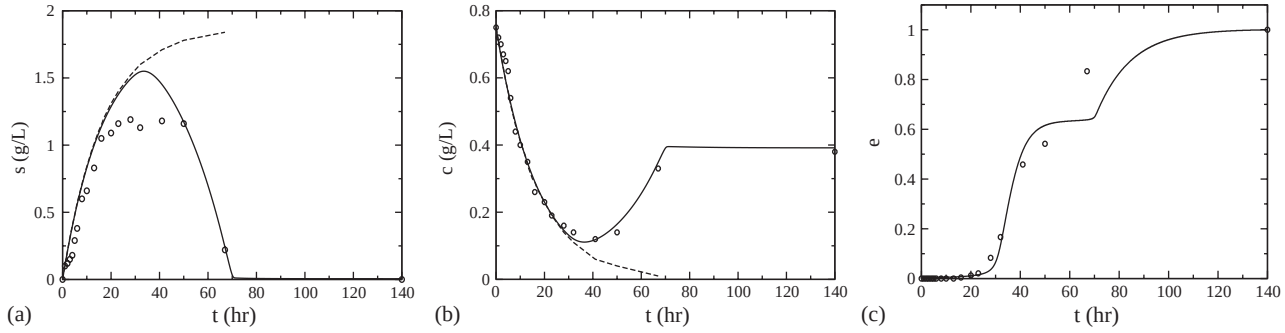

Fig. 1. Transient response of a *C. heintzii* culture to a switch in the identity of the growth-limiting substrate (data from Bally and Egli (1996), simulations of our earlier model (Shoemaker et al., 2003)). At $t<0$, the culture is growing on glucose at a dilution rate of 0.06 1/h. At $t=0$, the carbon source in the feed is switched from glucose to nitrilotriacetic acid (NTA), while the dilution rate is held fixed. (a) Concentration of NTA (b) Cell Density (c) Activity of NTA-monooxygenase scaled such that the maximum activity is 1. The dashed lines in (a) and (b) show the *theoretical washout curves*, i.e., the profiles that would be obtained in the absence of substrate consumption and growth, respectively. The close agreement between the theoretical washout curves and the experimental data for the first ~ 30 h implies that there is virtually no substrate uptake and growth during this period.

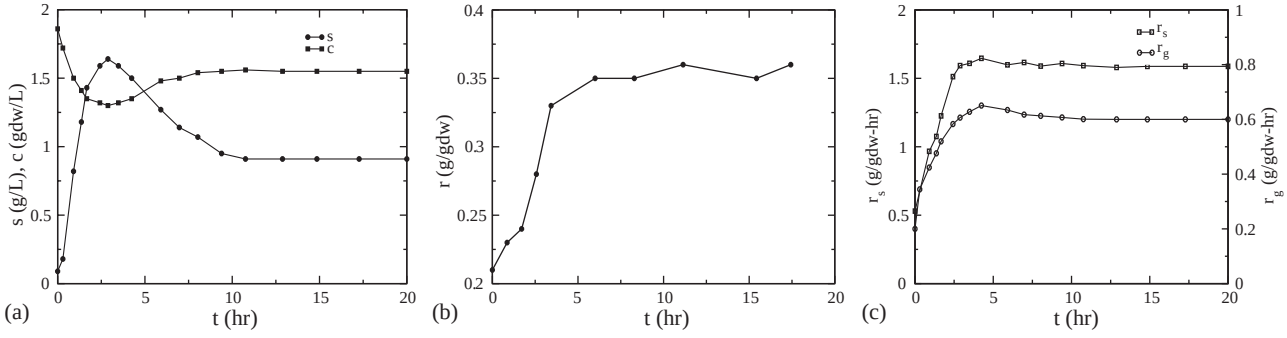

Fig. 2. Transient response of a glucose-limited culture of *E. coli* K12 to a dilution rate shift-up (from Yun et al., 1996). At $t<0$, the culture is at the steady-state corresponding to the dilution rate, $D_0 = 0.2\,1/\text{h}$, and feed concentration, $s_f = 5\,\text{g/L}$. At $t=0$, the dilution rate is shifted up to $D = 0.6\,1/\text{h}$, while the feed concentration is held constant. The figures show the evolution of the (a) Cell density and substrate concentration (b) Ribosome level (c) Specific substrate uptake and growth rates calculated from the curves in (a) by appealing to the formulas, $r_s = [D(s_f - s) - \mathrm{d}s/\mathrm{d}t]/c$ and $r_g = (\mathrm{d}c/\mathrm{d}t - Dc)/c$, which follow from the mass balances for the substrate and cells.

It is well known, however, that similar dynamics are observed even if the chemostat is subjected to *dilution rate shift-ups*. Indeed, when a glucose-limited culture of *E. coli* is subjected to a dilution rate shift-up, the cell density decreases and the substrate concentration increases (Fig. 2). But the steady-state peripheral enzyme levels are high at all $D > 0.1\,1/h$ (Fig. 3b). In fact, the enzyme levels are even higher than the levels observed at the maximum (washout) dilution rate. The existence of such high peripheral enzyme levels suggests that the dynamics of dilution rate shift-ups starting from sufficiently large initial dilution rates cannot be due to slow substrate uptake. What then is responsible for the sluggish response in such dilution rate shift-ups?

The source of the slow dynamics in dilution rate shift-ups is revealed by examining the initial response to *continuous-to-batch shifts*. In these experiments, cells maintained at steady state in a chemostat are abruptly exposed to excess substrate concentrations. The initial response is obtained by measuring the rates of various processes within 10–15 min of the shift to substrate-excess conditions. Fig. 4 shows the initial response of the substrate uptake, biosynthesis, respiration, and excretion in continuous-to-batch shifts of glucose-limited cells. It is evident that the specific substrate uptake rate increases to the maximal levels obtained near the washout dilution rate (Fig. 4a). However, the specific rate of RNA and protein synthesis increases only partially if the culture has been growing at low dilution rates, and shows no perceptible increase if the culture has been growing at high dilution rates (Fig. 4b). It follows that when cells growing at steady state in a chemostat are exposed to substrate-excess conditions, the substrate enters the cell at near-maximal rates, but the catabolic products derived from it are, at best, only partially channeled into biosynthesis. The excess substrate is eliminated by instantly increasing the rates of respiration (Fig. 4c), excretion (Fig. 4d), and storage (Harvey, 1970; Tempest et al., 1967). Thus, we conclude that the response is sluggish in dilution rate shift-ups because the specific RNA and protein synthesis rates do not achieve maximal levels instantly.

We wish to extend the model to account for these observations. Before attempting this, it must be asked why the specific RNA and protein synthesis rates fail to achieve maximal levels instantly. Clearly, some variable involved in the synthesis of RNA and proteins is limiting. The steady-state data suggests two possibilities. The biosynthetic enzyme, glutamate dehydrogenase (GDH), which supplies 80% of the amino acids in nitrogen-sufficient cultures (Reitzer and Magasanik, 1987) and the RNA (ribosome) levels, which catalyse the synthesis of protein from amino acids, are increasing functions of the dilution rate. It follows that in a dilution rate shift-up, the initial levels of GDH and ribosomes are lower than their final levels (Figs. 3b,c). This observation, by itself, does not explain the absence of the instantaneous increase in the specific growth rate. For, if these variables were subsaturated, the rapid increase in precursor levels would stimulate rapid synthesis of amino acids and proteins. However, if GDH or RNA are saturated with respect to their substrates, the desired result follows immediately.

1. If GDH is saturated, amino acid synthesis cannot be improved significantly until more GDH synthesized. In this case, the specific protein synthesis rate will be proportional to the activity of GDH throughout the transient following a continuous-to-batch shift.
2. If the ribosomes are saturated with amino acids, the protein synthesis rate remains at its pre-shift level until more ribosomes are synthesized, and the specific protein synthesis rate will be proportional to the ribosome level throughout a continuous-to-batch transient.

There is some evidence supporting the first hypothesis. Harvey has shown that the specific growth rate is proportional to the activity of GDH during the transient that follows a continuous-to-batch shift (Fig. 5a). On the other hand, several studies have shown that during

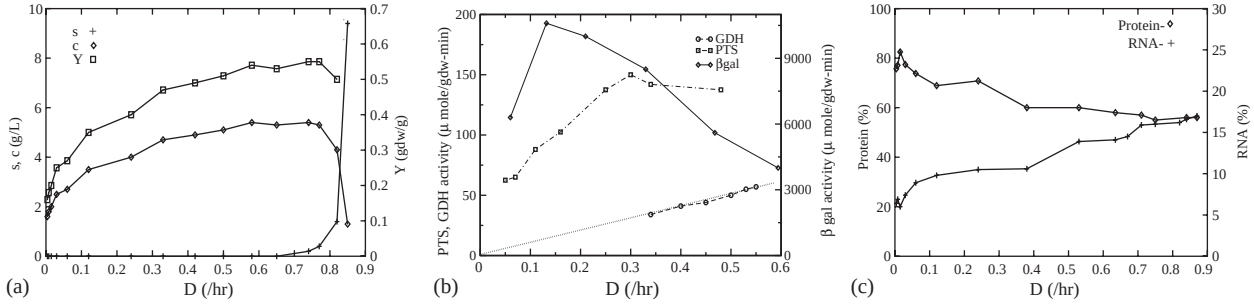

Fig. 3. Variation of steady states with respect to the dilution rate in carbon-limited cultures of *K. aerogenes*: (a) Cell density, substrate (glycerol) concentration and biomass yield (Tempest et al., 1967; Tempest and Hunter, 1965). (b) The peripheral enzyme levels pass through a maximum (data for β-galactosidase and phosphotransferase system (PTS) from Smith and Dean (1972) and Hunter and Kornberg (1979), respectively). The activity of the biosynthetic enzyme, glutamate dehydrogenase (GDH), increases monotonically (from Harvey, 1970). (c) The RNA content increases monotonically, while the protein content decreases monotonically (Tempest et al., 1967; Tempest and Hunter, 1965).

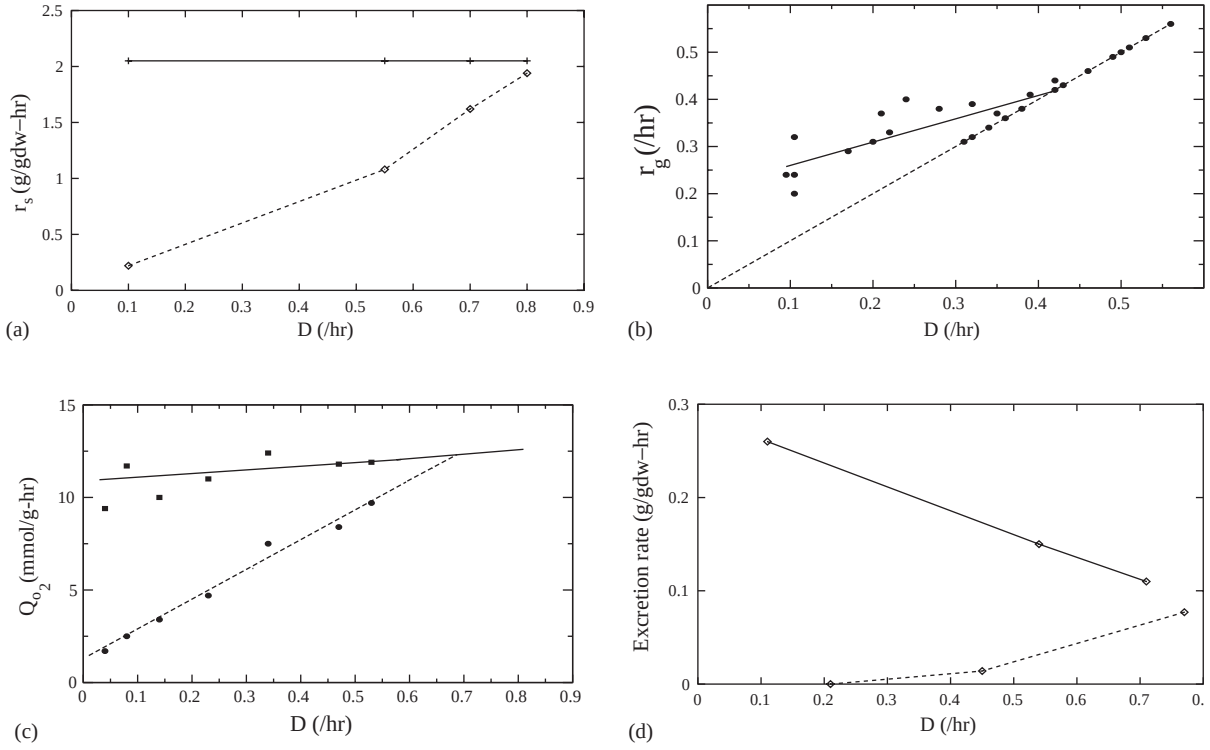

Fig. 4. Initial response of glucose-limited steady-state continuous cultures to supersaturating concentrations of glucose. The dashed line shows the rate of a process when the culture is in steady state at a particular dilution rate. The full line shows the rate of the same process immediately after the steady-state culture has been exposed to supersaturating concentrations of glucose. The data in (b) was obtained with glycogenless mutants of *E. coli* B at 30 °C. All other data was obtained with wild-type *K. aerogenes* at 37 °C. The data shows that immediately after exposure to substrate-excess conditions, the specific substrate uptake, respiration, and excretion rates jump to maximal or supramaximal levels. The specific rate of RNA and protein synthesis shows a partial increase at low dilution rates, and no perceptible increase at high dilution rates. (a) Substrate uptake rate (from O'Brien et al., 1980); (b) biosynthesis rate (from Harvey, 1970); (c) respiration rate (from Neijssel et al., 1977); (d) excretion rate (from Cooney et al., 1976; O'Brien et al., 1980).

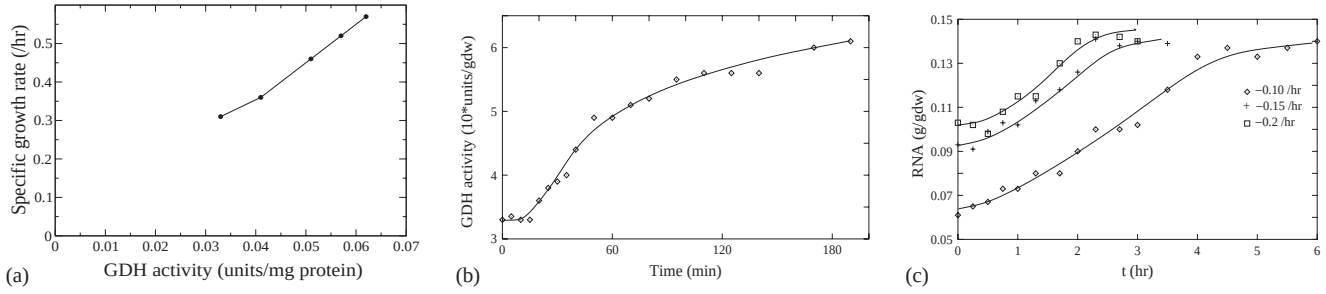

Fig. 5. Transient response of glucose-limited cultures to continuous-to-batch shifts: (a) The specific growth rate is proportional to GDH activity throughout the transient (Harvey, 1970). (b) The evolution of GDH activity has a sigmoidal profile (Harvey, 1970). (c) The evolution of RNA concentration also has a sigmoidal profile (Nagai et al., 1968). The three curves correspond to three different dilution rates.

the transients in substrate-excess conditions, the specific protein synthesis rate is proportional to the ribosome level (Brunschede et al., 1977; Maaloe and Kjeldgaard, 1966; Nielsen and Villadsen, 1992). In this work, we assume that biosynthesis is limited by ribosomes. A model accounting for both biosynthetic enyzmes and ribosomes is currently being investigated.

The initial response of continuous-to-batch shifts reveals the identity of the variables that prevent the biosynthesis rate from increasing instantly, but sheds no light on the reason for the slow response of these variables. We gain some insight into the mechanism of the slow response by examining the evolution of GDH and ribosome levels in continuous-to-batch shifts (Figs. 5b,c). These transients suggest that synthesis of GDH and ribosomes is autocatalytic. The synthesis rates are small initially, accelerate subsequently, and subside finally after passing through an inflection point. It is

conceivable that these autocatalytic kinetics occur because an increase in the activity of GDH results in elevated amino acid levels, which activate the synthesis of ribosomal RNA and ribosomes (Bremer and Dennis, 1975; Jensen and Pedersen, 1990; Zhang et al., 2002), thus stimulating the synthesis of even more GDH. As attractive as this hypothesis may be, the molecular mechanism by which amino acids stimulate RNA and ribosome synthesis remains a subject of some controversy. The debate is centered around the identity of the "messenger" molecules that communicate the availability of the amino acids to the machinery synthesizing the ribosomal RNA. Gourse and coworkers claim that the nucleotides (ATP, GTP) are the key messenger molecules (Gaal et al., 1997). Others have argued that ppGpp plays this role (Petersen and Moller, 2000; Zhang et al., 2002). In what follows, we assume that synthesis of RNA is autocatalytic without making any attempt to model the underlying molecular mechanism.

There are numerous models of continuous culture dynamics. In microbiology, the models have focused on the dynamics of RNA and protein synthesis (Bremer, 1975; Koch, 1970). These models assume that the protein synthesis rate is proportional to the concentration of RNA, and the RNA synthesis rate, in turn, is proportional to the concentration of proteins. This cycle of quasi-reactions implies that synthesis of RNA and proteins is, in effect, autocatalytic, which provides a mechanistic explanation for the slow response. In engineering, on the other hand, one is particularly interested in the dynamics of the substrate concentration and the cell density. Powell (1969) and Yun et al. (1996) formulated a simple model that yields a slow response, and also accounts for the variations of the substrate concentration and the cell density. Both models assume that the specific growth rate is proportional to RNA levels, and the specific substrate uptake rate is proportional to the specific growth rate. The slow responses are obtained by assuming that the synthesis rate of RNA is proportional to the concentration of RNA.[1] However, the assumption that substrate uptake and growth are coupled is inconsistent with experiments (Figs. 4a,b). Consequently, these models are unable to capture the cell density overshoot observed in dilution rate shift-downs (see Yun et al., 1996, Figure 6). Simulations of several detailed models that take due account of this uncoupling show good agreement with experimentally observed transients (Baloo and Ramkrishna, 1990; Domach et al., 1984; Nielsen and Villadsen, 1992), but the large number of variables prevents a precise analysis that would yield deeper insights. In this work, we formulate a detailed model accounting for the role of several intracellular variables. We show, however, that no more than 2 variables are relevant on the time scale of interest. This simplification allows us to perform a rigorous analysis that reveals the simple motifs underlying these dynamics. Specifically, we show that every transient is a combination of two basic dynamics typically observed in batch and fed-batch cultures. We show, furthermore, that the model captures and explain the data shown in Figs. 2–5 and additional data discussed below.

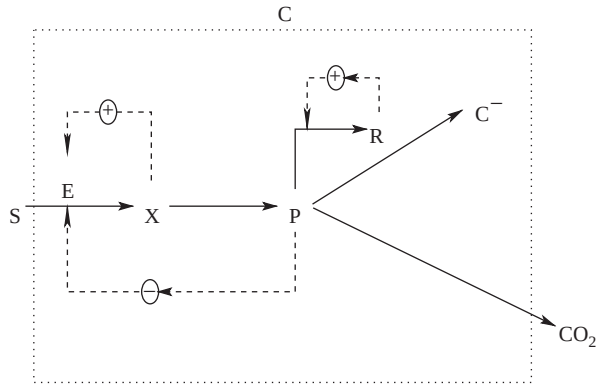

Fig. 6. Kinetic scheme of the model. Here, S denotes the substrate, E denotes the inducible enzyme(s) catalysing the uptake and peripheral catabolism of S, X denotes the inducer for E, P denotes the biosynthetic precursors derived from catabolism of X, R denotes rRNA, C^- denotes proteins, and C denotes the entire cell consisting of E, X, P, R, and C^-. The positive feedback loops represent induction of enzyme synthesis and autocatalytic synthesis of RNA. The negative feedback loop represents the inhibition of substrate uptake by precursors.

We begin by formulating the extended model (Section 2). We then simulate and analyse the model to show that it yields results in qualitative agreement with the data (Section 3). Finally, we discuss the extent to which the model captures the key results of the experimental literature (Section 4), and summarize the conclusions (Section 5).

2. The model

Fig. 6 shows the kinetic scheme of the model. Here, S denotes the growth-limiting carbon and energy source, E denotes the peripheral enzymes that catalyse the transport and peripheral catabolism of the carbon source and X denotes the internalized form of the substrate that induces the synthesis of E;[2] P denotes the pool of precursors produced by catabolism of X; R

[1]The model in Shoemaker et al. (2002) is formally similar to these models, the only difference being that it is the peripheral enzyme, rather than RNA, that is synthesized autocatalytically (Shoemaker et al., 2003).

[2]For example, if S is lactose, then E is any one of the three coordinately controlled enzymes of the *lac* operon and X is allolactose (Lin, 1987). Likewise, if S is glucose, then E is any of the enzymes of the phosphotransferase system (PTS) and X is phosphorylated glucose (Plumbridge, 2003).

denotes ribosomes or ribosomal RNA (rRNA);[3] and C^- denotes proteins. The entire cell consisting of E, X, P, R, and C^- is denoted by C. The term *biosynthesis* will be used to refer to the synthesis of RNA and proteins, and *growth* will refer to the synthesis of all intracellular components.

Throughout this work, the instantaneous concentrations of the variables are denoted by the corresponding lower-case letters s, e, x, p, r, c^-, and c, while steady state and quasisteady state concentrations are denoted by overlaying the letters with $\sim$ and $-$, respectively (for instance, $\tilde{x}$ and $\bar{x}$). The concentrations of the *environmental* variables, s and c, are based on the volume of chemostat (g/L and gdw/L, respectively), and the concentrations of the *physiological* variables, e, x, p, r, and c^- are based on the dry weight of biomass (g/gdw).

We make the following assumptions regarding the kinetics of the processes.

1. The specific substrate uptake rate, denoted r_s, satisfies the kinetic law

   $$r_s \equiv V_s e \frac{s}{K_s + s} \frac{1}{1 + p/K_i};$$

   where the factor $1/(1 + p/K_i)$ denotes the inhibition of substrate uptake by precursors. The experimental data suggests that such feedback inhibition exists. Indeed, if there were no feedback inhibition, the specific substrate uptake immediately after a continuous-to-batch shift would be proportional to the preexisting steady-state enzyme level ($\bar{r}_s \approx V_s \tilde{e}$). Since $\tilde{e}$ increases three-fold as D decreases from 0.6 l/h to 0.2 l/h (Fig. 3b), $\bar{r}_s$ should be three-fold higher for cultures growing at $D = 0.2$ l/h compared to cultures growing at $D = 0.6$ l/h. But Fig. 4a shows that $\bar{r}_s$ is the same for cultures growing at dilution rates between 0.2 and 0.6 l/h. This suggests that in cultures growing at low dilution rates, feedback inhibition acts to prevent the specific substrate rate from exceeding its value at high dilution rates.
2. The specific rate of breakdown of X into energy and precursors P, denoted r_x, is given by

   $$r_x \equiv k_x x.$$

3. The specific rate of respiration is

   $$r_{co_2} \equiv k_{co_2} p.$$

4. The specific rate of enzyme synthesis, denoted r_e^+, is

   $$r_e^+ \equiv V_e \frac{r}{K_e + r} \frac{1 + K_2 x^2}{K_3 + K_2 x^2}. \quad (1)$$

   Underlying these kinetics is the fact that the enzyme synthesis rate is precisely the rate at which the messenger RNA (mRNA) for the enzyme is translated by the ribosomes. We assume that the specific translation rate of the enzyme is $k_e m r/(K_e + r)$, where m and r denote the concentration of mRNA and ribosomes, respectively. Now, the evolution of mRNA is given by the equation $dm/dt = r_m^+ - r_m^- - r_g m$, where $r_m^+ \equiv V_m(1 + K_2 x^2)/(K_3 + K_2 x^2)$ is the specific transcription rate,[4] $r_m^- \equiv k_m^- m$ is the specific degradation rate, and $r_g m$ is the dilution rate. Since mRNA has a half-life of ~ 2 min ($k_m^- \approx 20$ l/h) (Gausing, 1977), it rapidly reaches the quasisteady state concentration, $\bar{m} \approx r_m^+/k_m^-$. Substituting this concentration in the expression for the specific translation rate yields (1) with $V_e \equiv k_e V_m/k_m^-$.
5. The specific rate of (ribosomal) RNA synthesis is given by

   $$r_r^+ \equiv k_r^+ r p,$$

   where the dependence on r reflects the assumption that rRNA synthesis is autocatalytic.
6. The specific rate of protein (C^-) synthesis is given by

   $$r_c^+ \equiv V_c r \frac{p}{K_c + p},$$

   where the dependence on r accounts for the fact that ribosomes catalyse protein synthesis.
7. The specific rates of peripheral enzyme, rRNA, and protein degradation, denoted r_e^-, r_r^-, and r_c^-, respectively, are given by

   $$r_e^- \equiv k_e^- e, \quad r_r^- \equiv k_r^- r, \quad r_c^- \equiv k_c^- c^-.$$

8. The synthesis of peripheral enzymes, rRNA and proteins depletes the pool of precursors. Likewise, their degradation replenishes the pool of precursors.

A mass balance on the state variables yields

$$\frac{ds}{dt} = D(s_f - s) - r_s c, \quad (2)$$

$$\frac{dc^-}{dt} = r_c^+ - r_c^- - \left(D + \frac{1}{c}\frac{dc}{dt}\right)c^-, \quad (3)$$

$$\frac{de}{dt} = r_e^+ - r_e^- - \left(D + \frac{1}{c}\frac{dc}{dt}\right)e, \quad (4)$$

[3] We use the terms ribosome and rRNA interchangeably. This is appropriate because synthesis of ribosomal RNA and ribosomes is tightly coupled through a negative feedback loop involving regulation of ribosomal protein synthesis (Nomura, 1984).

[4] These kinetics reflect the fact that transcription of the mRNA for the peripheral enzymes involves the binding of a repressor molecule to two inducer molecules (Yagil and Yagil, 1971). Thus, K_2 is the equilibrium constant for binding of a repressor to two inducer molecules, and K_3 is proportional to the equilibrium constant for binding of the repressor to the operator. Note that since repressor-operator binding is not perfect, K_3 is finite, so that mRNA is transcribed even in the absence of the inducer ($r_m^+|_{x=0} = (V_m/K_3) > 0$). This phenomenon is called *constitutive* enzyme synthesis.

$$\frac{dr}{dt} = r_r^+ - r_r^- - \left(D + \frac{1}{c}\frac{dc}{dt}\right)r, \tag{5}$$

$$\frac{dx}{dt} = r_s - r_x - \left(D + \frac{1}{c}\frac{dc}{dt}\right)x, \tag{6}$$

$$\frac{dp}{dt} = r_x - r_{co_2} - (r_c^+ - r_c^-) - (r_e^+ - r_e^-) - (r_r^+ - r_r^-) - \left(D + \frac{1}{c}\frac{dc}{dt}\right)p, \tag{7}$$

where s_f denotes the concentration of S in the feed, and D denotes the dilution rate. These equations define $(1/c)(dc/dt)$ implicitly in terms of the other derivatives. We can solve for $(1/c)(dc/dt)$ explicitly by observing that the mass fraction of all intracellular entities equals unity, i.e.

$$c^- + e + r + x + p = 1. \tag{8}$$

Hence, addition of Eqs. (3)–(7) yields

$$D + \frac{1}{c}\frac{dc}{dt} = r_s - r_{co_2} \tag{9}$$

which can be rewritten in the more familiar form

$$\frac{dc}{dt} = (r_g - D)c,$$

where r_g denotes the specific growth rate, and is defined as

$$r_g \equiv r_s - r_{co_2}. \tag{10}$$

Eqs. (9) and (10) imply that the last term in Eqs. (3)–(7) represents the dilution of the corresponding physiological concentration due to growth.

Thus, we arrive at

$$\frac{ds}{dt} = D(s_f - s) - r_s c, \tag{11}$$

$$\frac{dc}{dt} = (r_g - D)c, \tag{12}$$

$$\frac{dc^-}{dt} = r_c^+ - r_c^- - r_g c^-, \tag{13}$$

$$\frac{de}{dt} = r_e^+ - r_e^- - r_g e, \tag{14}$$

$$\frac{dr}{dt} = r_r^+ - r_r^- - r_g r, \tag{15}$$

$$\frac{dx}{dt} = r_s - r_x - r_g x, \tag{16}$$

$$\frac{dp}{dt} = r_x - r_{co_2} - (r_c^+ - r_c^-) - (r_e^+ - r_e^-) - (r_r^+ - r_r^-) - r_g p, \tag{17}$$

where r_g is given by Eq. (10). It is worth noting that Eq. (8) implies that Eqs. (13)–(17) are linearly dependent. Hence, we can replace any one of these equations with Eq. (8).

3. Simulations

The simulations were done with the parameter values in Table 1. The rationale for order-of-magnitude estimates of these parameters is given in Appendix A.

3.1. Steady states

To analyse the steady states, we replace Eq. (17) with Eq. (8). Thus, we consider

$$\frac{ds}{dt} = D(s_f - s) - \left(V_s e \frac{s}{K_s + s}\frac{1}{1 + p/K_i}\right)c = 0, \tag{18}$$

$$\frac{dc}{dt} = (r_g - D)c = 0, \tag{19}$$

$$\frac{dc^-}{dt} = V_c r \frac{p}{K_c + p} - (r_g + k_c^-)c^- = 0, \tag{20}$$

$$\frac{de}{dt} = V_e \frac{r}{K_e + r}\frac{1 + K_2 x^2}{K_3 + K_2 x^2} - (r_g + k_e^-)e = 0, \tag{21}$$

$$\frac{dr}{dt} = (k_r^+ p - r_g - k_r^-)r = 0, \tag{22}$$

$$\frac{dx}{dt} = V_s e \frac{s}{K_s + s}\frac{1}{1 + p/K_i} - (r_g + k_x)x = 0, \tag{23}$$

$$p = 1 - (c^- + e + r + x), \tag{24}$$

where r_g is given by Eq. (10). These equations admit three types of steady states—the *persistence* steady state ($\tilde{c} > 0, \tilde{r} > 0$), the *washout* steady state ($\tilde{c} = 0$, $\tilde{r} > 0$), and the *death* steady state ($\tilde{c} = 0$, $\tilde{r} = 0$). For a given microbial species and growth-limiting substrate, these steady states can depend on two parameters—the dilution rate and the feed concentration.

Table 1
Parameter values used in the simulations (see Appendix A for details)

$V_s = 2 \times 10^4$ g/g-h	$K_s = 10^{-2}$ g/L	$K_i = 5 \times 10^{-3}$ g/gdw	$k_x = 10^3$ g/g-h	$V_e = 5 \times 10^{-4}$ g/gdw-h
$K_e = 0.1$ g/gdw	$K_2 = 10^{10}$ (gdw/g)^2	$K_3 = 5 \times 10^3$	$k_e^- = 0.075$ g/g-h	$k_r^+ = 100$ gdw/g-h
$k_r^- = 0.1$ g/g-h	$V_c = 3$ g/g-h	$K_c = 0.002$ g/gdw	$k_c^- = 0.05$ g/g-h	$k_{co_2} = 150$ g/g-h

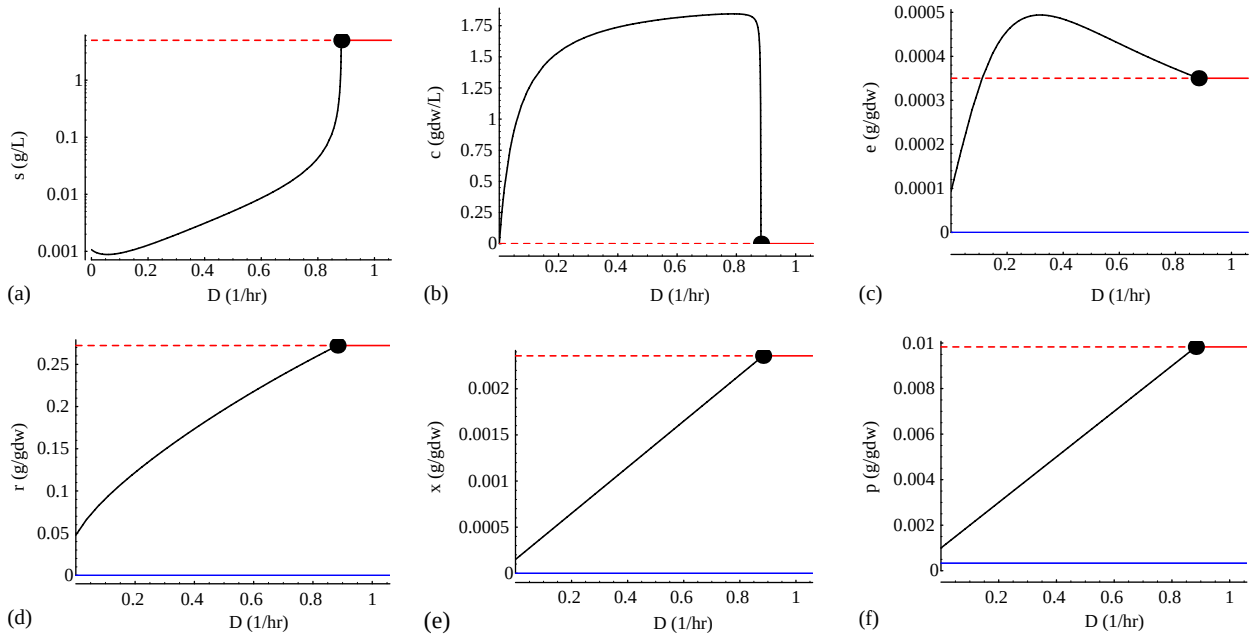

Fig. 7. Variation of the steady states with D at $s_f = 5$ g/l. The persistence, washout, and the (stable) death steady states are represented by black, red, and blue lines, respectively. Stable and unstable steady states are denoted by full and dashed lines, respectively. The full circle shows the bifurcation point at which the persistence and washout steady state exchange stability. The stable death steady state is not shown in (a) and (b) since it overlaps with the washout steady state.

3.1.1. *Persistence steady state*

The variation of the persistence steady state with respect to the feed concentration is simple. If the feed concentration is increased at a fixed dilution rate, the cell density increases, but there is no perceptible change in the substrate concentration (Grady et al., 1972; Senn et al., 1994). There is no data on the variation of the physiological steady states with respect to the feed concentration. However, since the physiological state is completely determined by the substrate concentration, these steady states should also be independent of the feed concentration. We show below that this property is inherent in the model.

The variation of the persistence steady state with respect to the dilution rate is more complex. The substrate concentration and ribosome levels increase monotonically (Figs. 3a,d). On the other hand, the cell density and peripheral enzyme levels pass through a maximum (Figs. 3b,c). Fig. 7 shows that the model simulations are in good agreement with this data. In what follows, we shed more light on these simulations by deriving explicit expressions for the steady-state values of all the variables.

To this end, observe that since $\tilde{c}, \tilde{r} > 0$ at the persistence steady state, Eqs. (19) and (22) imply that $\tilde{r}_g = D$ and

$$\tilde{p}(D) = \frac{D + k_r^-}{k_r^+}. \tag{25}$$

Thus, $\tilde{p}$ increases linearly with D (Fig. 7f). Interestingly, as D tends to zero, $\tilde{p}$ approaches a positive limit. Thus, we obtain "maintenance effects," even though no maintenance was explicitly postulated. Indeed, substituting Eq. (25) in Eq. (10) yields

$$\tilde{r}_s = D + \tilde{r}_{co_2} = D + k_{co_2}\tilde{p} = D + k_{co_2}\left(\frac{D + k_r^-}{k_r^+}\right) = \frac{D}{\hat{Y}} + m, \tag{26}$$

where $\hat{Y} \equiv k_r^+/(k_r^+ + k_{co_2})$ is the *maximum yield of biomass*, and $m \equiv k_{co_2}(k_r^-/k_r^+)$ is the *maintenance coefficient* (which reflects the "futile cycling" of rRNA at vanishingly small dilution rates).

It follows immediately from Eqs. (23) and (26) that

$$\tilde{x}(D) = \frac{\tilde{r}_s}{k_x + D} = \frac{D/\hat{Y} + m}{k_x + D} \approx \frac{D/\hat{Y} + m}{k_x} \tag{27}$$

so that $\tilde{x}$ increases linearly with the dilution rate (Fig. 7e). To find the concentrations of the remaining physiological variables, we observe that Eqs. (20) and (21) imply that[5]

$$\tilde{c}^-(\tilde{r}) = \frac{\tilde{r}_c^-}{D + k_c^-} = \frac{V_c}{D + k_c^-}\tilde{r}\frac{\tilde{p}}{K_c + \tilde{p}},$$
$$\tilde{e}(\tilde{r}) = \frac{\tilde{r}_e^+}{D + k_e^-} = \frac{V_e}{D + k_e^-}\frac{\tilde{r}}{K_e + \tilde{r}}\frac{1 + K_2\tilde{x}^2}{K_3 + K_2\tilde{x}^2}. \tag{28}$$

[5]The first relation in Eq. (28) implies that at steady state

$$\frac{\tilde{r}}{\tilde{c}^-} = \frac{D + k_c^-}{V_c\tilde{p}/(K_c + \tilde{p})},$$

where the denominator represents the protein synthesis rate per unit ribosome, often referred to as the *peptide chain growth rate* in the microbiological literature. At high dilution rates, $D \gg k_c^-$ and

Substituting these relations in Eq. (24) yields

$$\tilde{r}+\frac{V_c}{D+k_c^-}\tilde{r}\frac{\tilde{p}}{K_c+\tilde{p}}+\frac{V_e}{D+k_e^-}\frac{\tilde{r}}{K_e+\tilde{r}}\frac{1+K_2\tilde{x}^2}{K_3+K_2\tilde{x}^2} = 1-\tilde{x}-\tilde{p} \quad (29)$$

which is a quadratic in $\tilde{r}$. Since the LHS is an increasing function of $\tilde{r}$, and the RHS is independent of $\tilde{r}$, Eq. (29) has at most one positive root at any given D. A simple approximation to $\tilde{r}(D)$ is obtained by recognizing that $\tilde{e},\tilde{x},\tilde{p}\ll 1$. In this case, Eq. (29) yields the relation

$$\frac{\tilde{r}}{1-\tilde{r}}\approx\frac{\tilde{r}}{\tilde{c}^-}=\frac{D+k_c^-}{V_c}\frac{K_c+\tilde{p}}{\tilde{p}} = \frac{k_r^+}{V_c}\frac{D+k_c^-}{D+k_r^-}(K_c+\tilde{p}). \quad (30)$$

At high dilution rates, $D\gg k_c^-,k_r^-$ and protein synthesis is saturated ($p\gg K_c$), so that

$$\frac{\tilde{r}}{1-\tilde{r}}\approx\frac{\tilde{r}}{\tilde{c}^-}=\frac{D}{V_c+D}$$

which implies that $\tilde{r}$ increases (and $\tilde{c}^-$ decreases) with D (Fig. 7d). The steady-state enzyme level is obtained by substituting $\tilde{r}(D)$ in Eq. (28). It passes through a maximum since the enzyme synthesis rate saturates at large D, i.e., $\tilde{r}_e^+\approx V_e$ (Fig. 7c).

The steady-state substrate concentration can be derived by appealing to the definition of r_s. Thus

$$\frac{\tilde{s}}{K_s+\tilde{s}}=\frac{\tilde{r}_s}{V_s\tilde{e}/(1+\tilde{p}/K_i)}. \quad (31)$$

We gain some insight into the variation of $\tilde{s}$ with respect to D (Fig. 7a) by recalling that $\tilde{r}_s$ and $\tilde{p}$ increase linearly with D. At high dilution rates, $\tilde{e}\approx V_e/D$, so that $\tilde{s}/(K_s+\tilde{s})$, and hence, $\tilde{s}$, increases with D.

The variation of the steady-state cell density with D (Fig. 7b) follows immediately from Eq. (18). Thus

$$\tilde{c}=\frac{D(s_f-\tilde{s})}{\tilde{r}_s}. \quad (32)$$

At low dilution rates, $\tilde{s}\ll s_f$ and $\tilde{r}_s\approx m$; hence, $\tilde{c}\approx(s_f/m)D$. At high dilution rates, $\tilde{r}_s\approx D/\hat{Y}$, so that $\tilde{c}\approx\hat{Y}(s_f-\tilde{s})$.

Note that the steady-state concentrations of the substrate and the physiological variables are independent of the feed concentration, s_f. This is because the steady-state concentrations of S and the five physiological variables (C^-, E, R, X, and P) are completely determined by the six equations (19)–(24), which are independent of the feed concentration.

3.1.2. Washout steady state

As noted above, at high dilution rates, the substrate concentration corresponding to the persistent steady state is an increasing function of D. When D becomes sufficiently large, $\tilde{s}=s_f$ and $\tilde{c}=0$, i.e., the cells wash out of the chemostat. We refer to this steady state as the *washout steady state*, and the corresponding dilution rate, denoted D_w, as the *washout dilution rate*. The physiological variables corresponding to this steady state are determined by Eqs. (20)–(24) with $r_g=r_s-r_{co_2}$ and $\tilde{s}=s_f$. It follows that the washout steady state is independent of the dilution rate.

Since the washout steady state is achieved when the substrate concentration corresponding to the persistent steady state equals s_f, the washout dilution rate satisfies the following equation obtained by letting $\tilde{s}=s_f$ in Eq. (31):

$$\frac{s_f}{K_s+s_f}=\frac{\tilde{r}_s}{V_s\tilde{e}/(1+\tilde{p}/K_i)}, \quad (33)$$

where $\tilde{p}$, $\tilde{r}_s$, and $\tilde{e}$ are given by Eqs. (25), (26) and (28), respectively. Now, in typical experiments, $s_f\sim 1\,\mathrm{g/L}$, so that $s_f/(K_s+s_f)\approx 1$. Moreover, at large dilution rates ($D\approx D_w$), $\tilde{p}$, $\tilde{r}_s$, and $\tilde{e}$ can be approximated by the relations

$$\tilde{p}\approx\frac{D}{k_r^+},\quad \tilde{r}_s\approx\frac{D}{\hat{Y}},\quad \tilde{e}\approx\frac{V_e}{D}$$

since the loss of enzyme and rRNA by degradation is negligible compared to their loss by dilution due to growth ($k_e^-,k_r^-\ll D$); substrate consumption for maintenance (as opposed to growth) is negligibly small ($m\ll D/\hat{Y}$); and enzyme induction is near-maximal ($r_e^+\approx V_e$). We substitute these relations in Eq. (33) to conclude that the washout dilution rate satisfies the approximate relation

$$\frac{1}{k_r^+K_i}D_w^3+D_w^2\approx\hat{Y}V_sV_e,$$

which has a unique positive solution. In the absence of feedback inhibition ($K_i\to\infty$), we obtain a simple approximation, $D_w\approx\sqrt{\hat{Y}V_sV_e}$, which provides a convenient upper bound for the washout dilution rate.

3.1.3. Death steady states

A death steady state is characterized by the condition, $\tilde{r}=0$. We refer to this as the death steady state for the following reason. When the cells are starved of one or more nutrients, they degrade preexisting RNA and proteins to precursors, which are then oxidized to generate the energy required for maintenance (Kaplan

(*footnote continued*)
$V_c\tilde{p}/(K_c+\tilde{p})\approx V_c$ so that $\tilde{r}/\tilde{c}^-$ increases linearly with the dilution rate. This relationship has been observed in numerous organisms, and has led to the suggestion that there must a regulatory mechanism, given the name *growth rate control*, that ensures that the ribosome levels increase in proportion to the growth rate (Roberts, 1997). Despite 4 decades of intense efforts, no mechanism has been discovered. According to our model, the linear relationship is a simple consequence of the fact that ribosomes catalyse protein synthesis, and the chain growth rate saturates at high dilution rates.

and Apirion, 1975). If starvation persists for a sufficiently long time, the RNA level approaches zero, synthesis of proteins and enzymes ceases, and the cells die (Davis et al., 1986).

The death steady states satisfy

$$\frac{ds}{dt} = D(s_f - s) - r_s c = 0, \tag{34}$$

$$\frac{dc}{dt} = (r_g - D)c = 0, \tag{35}$$

$$\frac{dc^-}{dt} = -(k_c^- + r_g)c^- = 0, \tag{36}$$

$$\frac{de}{dt} = -(k_e^- + r_g)e = 0, \tag{37}$$

$$\frac{dx}{dt} = r_s - (k_x + r_g)x = 0, \tag{38}$$

$$1 = c^- + e + x + p. \tag{39}$$

At a death steady state, $\tilde{r}_g \leqslant 0$, because Eq. (37) implies that either $\tilde{r}_g = -k_e < 0$ or $\tilde{e} = 0$, but in the latter case, $\tilde{r}_s = 0$ and $\tilde{r}_g \equiv \tilde{r}_s - \tilde{r}_{co_2} = -k_{co_2}\tilde{p} \leqslant 0$. Hence, Eqs. (34)–(35) imply that $\tilde{c} = 0$ and $\tilde{s} = s_f$ at a death steady state. Thus, we are left with a system of four equations (36)–(39). We will assume henceforth that the rates k_c^-, k_e^-, k_x, k_{co_2} are pairwise distinct. It is now easy to see that there are only four possible cases

- (A) $\tilde{c}^- > 0$, $\tilde{r}_g = -k_c^-$. In this case, $\tilde{e} = 0 \to \tilde{r}_s = 0 \to \tilde{x} = 0$. Since $-k_c^- = \tilde{r}_g = -k_{co_2}\tilde{p}$, we have that
$$\tilde{p} = \frac{k_c^-}{k_{co_2}}, \quad c^- = 1 - \frac{k_c^-}{k_{co_2}}.$$
This steady state is therefore feasible[6] if and only if $k_c^- < k_{co_2}$.
- (B) $\tilde{e} > 0$, $\tilde{r}_g = -k_e$. In this case, $c^- = 0$. Furthermore,
$$0 \leqslant r_s = (k_x + \tilde{r}_g)\tilde{x} = (k_x - k_e^-)\tilde{x} = k_{co_2}\tilde{p} - k_e^-.$$
Thus we can express
$$\tilde{x} = \frac{k_{co_2}\tilde{p} - k_e^-}{k_x - k_e^-}.$$
Using the functional form of $\tilde{r}_s$, we find that
$$e = \frac{\tilde{r}_s(1 + \tilde{p}/K_i)}{V_s\sigma_f} = \frac{(k_{co_2}\tilde{p} - k_e^-)(1 + \tilde{p}/K_i)}{V_s\sigma_f}.$$
Equation $x + e + p = 1$ now takes the form
$$\frac{(k_{co_2}\tilde{p} - k_e^-)(1 + \tilde{p}/K_i)}{V_s\sigma_f} + \frac{k_{co_2}\tilde{p} - k_e^-}{k_x - k_e^-} + \tilde{p} = 1. \tag{40}$$
The left-hand side of Eq. (40) is increasing in $\tilde{p}$, thus at most one solution is possible. We conclude that case B is feasible if and only if $k_e^- < \min(k_x, k_{co_2})$.
- (C) $\tilde{c}^- = \tilde{e} = 0$, $\tilde{x} > 0$, $\tilde{r}_g = -k_x$. Since $\tilde{r}_s = 0$, we have that $-k_x = -k_{co_2}\tilde{p}$, and thus
$$\tilde{p} = \frac{k_x}{k_{co_2}}, \quad \tilde{x} = 1 - \frac{k_x}{k_{co_2}}.$$
This case is feasible if and only if $k_x < k_{co_2}$.
- (D) $\tilde{c}^- = \tilde{e} = \tilde{x} = 0$, $\tilde{p} = 1$, and $\tilde{r}_g = -k_{co_2}$. This case is always feasible.

For the parameter values in Table 1, only cases A, B, and D are feasible.

The stability analysis of these steady states is shown in Appendix B. This analysis shows that case D is always unstable. Of the two remaining steady states (cases A and B), one is always stable and the other is always unstable. For the parameter values in Table 1, case A is always stable, whereas cases B and D are always unstable.

3.2. Transients

To simulate and analyse the transients, we replace Eq. (13) with Eq. (8). Thus, we consider the equations.

$$\frac{ds}{dt} = D(s_f - s) - r_s c,$$

$$\frac{dc}{dt} = (r_g - D)c,$$

$$\frac{de}{dt} = r_e^+ - r_e^- - r_g e,$$

$$\frac{dr}{dt} = r_r^+ - r_r^- - r_g r,$$

$$\frac{dx}{dt} = r_s - r_x - r_g x,$$

$$\frac{dp}{dt} = r_x - r_{co_2} - (r_c^+ - r_c^-) - (r_e^+ - r_e^-) - (r_r^+ - r_r^-) - r_g p,$$

$$c^- = 1 - e - r - x - p.$$

It is shown in Appendix C that for all but a negligibly small time interval, these equations can be approximated by the *reduced* equations

$$\frac{ds}{dt} = D(s_f - s) - \left(V_s e \frac{s}{K_s + s}\frac{1}{1 + \bar{p}/K_i}\right)c, \tag{41}$$

$$\frac{dc}{dt} = (r_g - D)c, \tag{42}$$

$$\frac{de}{dt} = V_e \frac{r}{K_e + r}\frac{1 + K_2\bar{x}^2}{K_3 + K_2\bar{x}^2} - k_e^- e - r_g e, \tag{43}$$

[6] Feasibility refers to the fact that all physiological state variables are nonnegative. In particular, the specific substrate uptake rate r_s must be nonnegative. On the contrary, the specific growth rate r_g may be positive or negative.

$$\frac{dr}{dt} = k_r^+ r\bar{p} - k_r^- r - r_g r, \tag{44}$$

$$0 \approx V_s e \frac{s}{K_s + s} \frac{1}{1 + \bar{p}/K_i} - k_x \bar{x}, \tag{45}$$

$$0 \approx k_x \bar{x} - k_{co_2}\bar{p} - r_g, \tag{46}$$

where r_g is given by

$$r_g \approx V_c r \frac{\bar{p}}{K_c + \bar{p}} - k_c^-(1 - r) + k_r^+ r\bar{p} - k_r^- r. \tag{47}$$

That is, the specific growth rate is effectively equal to the specific rate of net rRNA and protein biosynthesis.

3.2.1. Continuous-to-batch shifts

In continuous-to-batch shifts, the initial rates of various processes are measured within 10–15 min of exposing the culture to substrate-excess conditions (Fig. 4). To simulate these experiments with the model, we observe that in this short time period, the peripheral enzyme and ribosome levels remain essentially unchanged, but the inducer and precursor concentrations rapidly move to the new quasisteady state corresponding to substrate-excess conditions. This new quasisteady state is obtained by letting $s/(K_s + s) \approx 1$ in Eqs. (45)–(46), while the peripheral enzyme and ribosome levels are held at their initial steady-state values, $e_0 = \tilde{e}(D)$ and $r_0 = \tilde{r}(D)$. Thus

$$\bar{x} \approx \frac{V_s e_0/(1 + \bar{p}/K_i)}{k_x} \tag{48}$$

and $\bar{p}$ satisfies

$$V_s e_0 \frac{1}{1 + \bar{p}/K_i} \approx k_{co_2}\bar{p} + V_c r_0 \frac{\bar{p}}{K_c + \bar{p}} - k_c^-(1 - r_0) + k_r^+ r_0 \bar{p} - k_r^- r_0. \tag{49}$$

If we assume that the degradation rates of rRNA and protein are negligibly small compared to their synthesis rates, and protein synthesis is saturated ($\bar{p} \gg K_c$), Eq. (49) can be solved to yield the approximate solution

$$\bar{p} \approx \frac{K_i}{2}\left(\sqrt{\left(1 + \frac{V_c r_0}{(k_{co_2} + k_r^+ r_0)K_i}\right)^2 + 4\frac{V_s e_0 - V_c r_0}{(k_{co_2} + k_r^+ r_0)K_i}} - \frac{V_c r_0}{(k_{co_2} + k_r^+ r_0)K_i}\right) \tag{50}$$

which is accurate to within 10% of the exact (numerical) solution for all e_0 and r_0. The rates of various processes immediately after a continuous-to-batch shift can now be obtained by substituting the above concentrations into the appropriate kinetic expressions (for example, $\bar{r}_s = V_s e_0/(1 + \bar{p}/K_i)$ and $\bar{r}_{co_2} = k_{co_2}\bar{p}$).

Fig. 8 shows the rates of various processes and the quasisteady state concentrations ($\bar{x}$,$\bar{p}$) immediately after the continuous-to-batch shift. The simulated rates are consistent with the experimental data shown in Fig. 4. At all but the smallest dilution rates, the specific substrate uptake and respiration rates immediately jump to high levels (Fig. 8a,b), but the specific growth rate increases only partially (Fig. 8c). Thus, substrate uptake and growth become uncoupled immediately after the shift, resulting in a reduction of the instantaneous yield, $Y \equiv r_g/r_s$ (Fig. 8d). The increase in the specific substrate uptake and growth rates is largest at intermediate dilution rates, and decreases at low and high dilution rates. At high dilution rates, substrate uptake is already saturated before the cells are exposed to substrate-excess conditions ($s_0 \gg K_s$), so that further provision of the substrate provokes no additional response. At low dilution rates, the initial peripheral enzyme are too

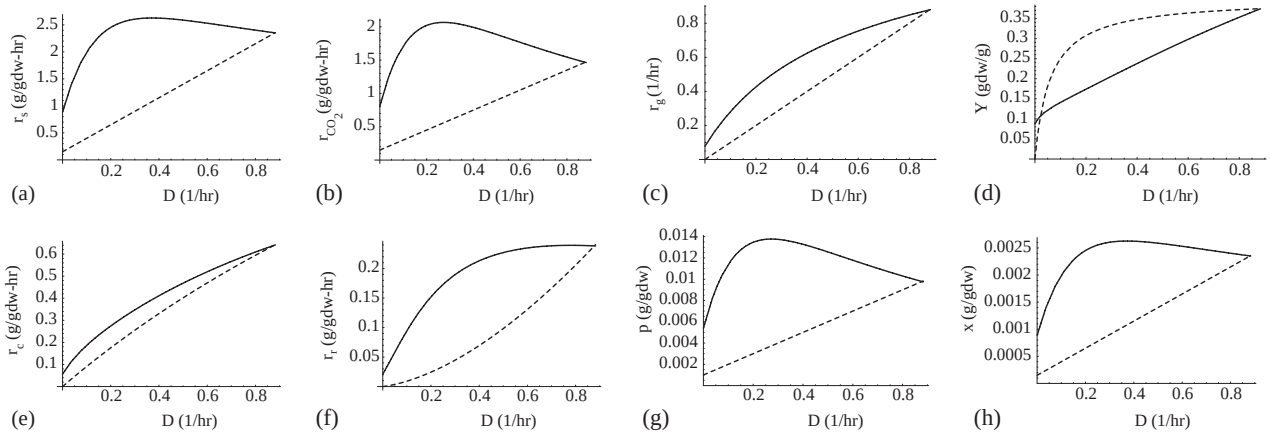

Fig. 8. Initial response following a continuous-to-batch shift. The dashed line shows the initial steady state value. The full line shows the value after the cells have been exposed to substrate-excess conditions: (a) Specific substrate uptake rate (b) Specific respiration rate (c) Specific growth rate (d) Yield of biomass (e) Net specific protein synthesis rate ($r_c \equiv r_c^+ - r_c^-$) (f) Net specific rRNA synthesis rate ($r_r \equiv r_r^+ - r_r^-$) (g) Precursor concentration (h) Inducer concentration.

small to support a substantial increment in the specific substrate uptake rate, and the initial rRNA levels are too small to support a substantial increment in the protein and rRNA synthesis rates (Figs. 8e,f).

3.2.2. Substrate switch

The transient response to substrate switches could be captured by our earlier model (see Fig. 1). Simulations of the extended model preserve these transients. The specific substrate uptake and growth rates remain at vanishingly small levels for the first ~ 20 h (Figs. 9c,f). Consequently, the substrate concentration and cell density go through a massive overshoot and undershoot, respectively (Figs. 9a,b). The peripheral enzyme level shows a biphasic response: After an initial increase, it becomes more or less constant at $t \approx 25$ h before increasing once again (Fig. 9d). These simulations are in good agreement with the data shown in Fig. 1. In addition to these dynamics, the extended model also describes the evolution of rRNA (Fig. 9e).

We can decompose these dynamics into four phases. It is worth examining these phases in more detail. As we show later, the dynamics of dilution rate shift-ups and shift-downs reproduce the dynamics of one or more of these phases.

Phase 1: During the *first* phase, the substrate attains supersaturating concentrations within 10–15 min. Indeed, since the initial enzyme level is negligibly small $[e_0 = (V_e/K_3)(D + k_e^-)r_0/(K_e + r_0) \sim 10^{-6}$ g/gdw], so is the initial substrate uptake rate. The initial motion of the substrate concentration is, therefore, approximated by

$$\frac{ds}{dt} \approx Ds_f - Ds, \quad s(0) = 0$$
$$\Rightarrow s(t) \approx s_f[1 - \exp(-Dt)]. \tag{51}$$

This equation describes the theoretical washout curve shown as a dashed curve in Fig. 4a. It implies that the substrate concentration increases to supersaturating levels ($s \sim K_s$) within

$$-\frac{\ln(1 - K_s/s_f)}{D} \approx \frac{K_s/s_f}{D} \sim 0.1 \text{ h}.$$

On this short time-scale, the cell density, the peripheral enzyme level, and the ribosome level remain at their initial values, but the inducer and precursor concentrations constantly adjust to the rapidly increasing substrate concentration. Hence, at the end of this phase, $c = c_0$, $e = e_0$, $r = r_0$, but s reaches supersaturating levels, and x, p achieve the corresponding quasisteady state concentrations given by Eqs. (48) and (50).

Phase 2: During the *second* phase, which lasts about 30 h, the substrate concentration is supersaturating, i.e., $s/(K_s + s) \approx 1$. Under these conditions, the substrate concentration and cell density change, but these changes cannot be discerned by the cells, since they see the environment through the ratio $s/(K_s + s)$, and this ratio is approximately constant. Given this quasiconstant environment, the physiological variables evolve toward a quasisteady state. We shall refer to this transient as *substrate-sufficient batch dynamics* because the quasisteady state reached by the physiological variables is identical to the physiological state attained by a

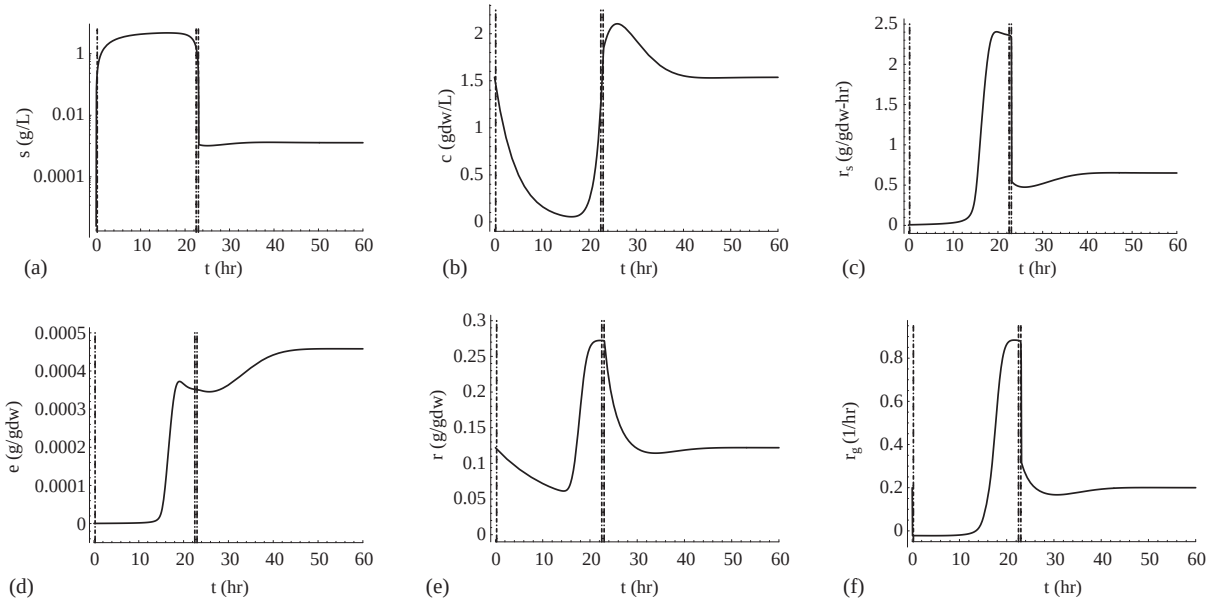

Fig. 9. Trajectories for a switch in the identity of the substrate at $D = 0.21$/h. Before the switch, the culture is in a steady state corresponding to the absence of the substrate. The vertical dashed lines mark the end of Phases 1, 2 and 3.

substrate-sufficient batch culture during the exponential growth phase: All the physiological variables are constant, and the cells grow exponentially at their maximum specific growth rate (Fig. 9f). In the microbiological literature, this quasisteady state is frequently referred to as the state of *balanced growth.*

The simulations show that during the approach to balanced growth, the enzyme and ribosome levels accumulate, pass through a maximum, and finally reach the constant level characteristic of balanced growth. To gain further insight into this transient, we observe that throughout the approach to balanced growth, the substrate concentration is supersaturating, so that the inducer and precursor levels are in the quasisteady state given by

$$\bar{x} \approx \frac{V_s e/(1+\bar{p}/K_i)}{k_x},$$

$$\bar{p} \approx \frac{K_i}{2}\left(\sqrt{\left(1+\frac{V_c r}{(k_{co_2}+k_r^+ r)K_i}\right)^2 + 4\frac{V_s e - V_c r}{(k_{co_2}+k_r^+ r)K_i}} - \frac{V_c r}{(k_{co_2}+k_r^+ r)K_i}\right). \quad (52)$$

The motion toward balanced growth is, therefore, two dimensional: The slow variables, e and r, evolve gradually according to Eqs. (43)–(44), while the fast variables, x and p, constantly adjust to the slow motion in accordance with Eq. (52). Fig. 10a shows the phase portrait for this two-dimensional motion. Note that

- The phase path intersects both null-clines before reaching balanced growth. Hence, both e and r pass through extrema on their way to balanced growth. Indeed, the eigenvalues of the linearization about the quasisteady state corresponding to balanced growth are imaginary with negative real parts ($\lambda_{1,2} = -1.1 \pm 0.5i$). The quasisteady state is, therefore, a stable focus, i.e., the phase path spirals into the quasisteady state.
- When the phase path crosses the null-cline for e (resp. r), the sign of $\dot{e}$ (resp. $\dot{r}$) changes from positive to negative. This implies that both e and r pass through a maximum before reaching balanced growth.
- The phase path intersects the null-cline for e before it intersects the null-cline for r. It follows that e reaches its maximum before r.

These dynamics reflect the fact that the specific enzyme synthesis rate increases first, followed by the specific ribosome synthesis rate, the specific protein synthesis rate, and finally, the specific growth rate. Thus, the peripheral enzyme and ribosome levels go through maxima because their synthesis rates increase too much before their dilution rates catch up, and the peripheral enzyme level reaches its maximum before the ribosome level because the synthesis rate of the enzyme increases before the synthesis rate of the ribosomes.

Phase 3: During the *third* phase, the substrate concentration switches from supersaturating to subsaturating levels. This transition, which marks the end of balanced growth, occurs on a time-scale of 1 min. To see this, observe that at the beginning of this phase, the substrate concentration is on the order of K_s, and the substrate uptake rate, $r_s c$, is on the order of 1 g/(L-h). It follows that within $K_s/(r_s c) \sim 0.01$ h of the end of balanced growth, the substrate reaches the quasisteady state concentration defined by

$$r_s c \approx D s_f. \quad (53)$$

At the same time, the inducer and precursor levels, which constantly adjust to the exogenous substrate concentration, achieve the corresponding

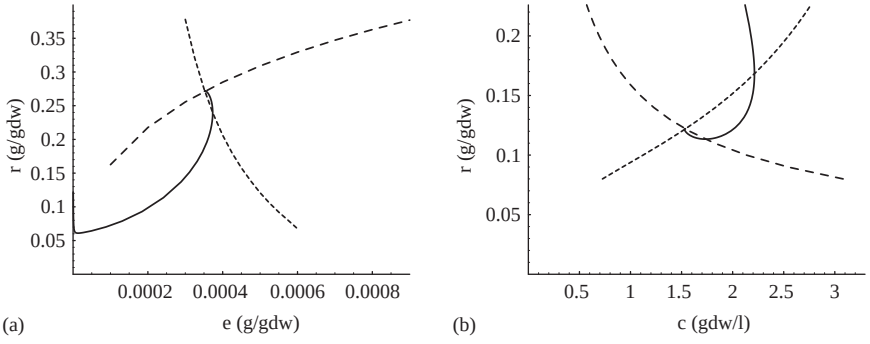

Fig. 10. Phase portraits of the slow motion during a feed switches. (a) The slow motion toward balanced growth. The line with short dashes shows the null-cline for e; the line with long dashes shows the null-cline for r; the intersection of the two null-clines represents the concentration of e and r at balanced growth; the full line shows the approach of e and r toward the state of balanced growth. (b) The slow motion away from balanced growth to the ultimate steady state. The line with short dashes shows the null-cline for c; the line with long dashes shows the null-cline for r; the intersection of the two null-clines represents the steady state concentrations of c and r at $D = 0.2$ l/h; and the full line shows the motion of c and r from balanced growth toward the final steady state.

quasisteady state values

$$\bar{x} \approx \frac{Ds_f/c}{k_x},$$

$$\bar{p} \approx \frac{K_c}{2}\left[\frac{Ds_f/c - V_c r}{(k_{co_2} + k_r^+ r)K_c} - 1 + \sqrt{\left(\frac{Ds_f/c - V_c r}{(k_{co_2} + k_r^+ r)K_c} - 1\right)^2 + 4\frac{Ds_f/c}{(k_{co_2} + k_r^+ r)K_c}}\right] \tag{54}$$

obtained by substituting Eq. (53) in Eqs. (45)–(46). The achievement of these quasisteady states is so rapid that the cell density, the peripheral enzyme level and the ribosome level remain at the values achieved at the end of balanced growth.

Phase 4: During the *last* phase, s, x and p remain in the quasisteady states defined by Eqs. (53)–(54), while e, r, and c evolve slowly according to

$$\frac{de}{dt} \approx V_e \frac{r}{K_e + r}\frac{1 + K_2\bar{x}^2}{K_3 + K_2\bar{x}^2} - k_e^- e - r_g e, \tag{55}$$

$$\frac{dr}{dt} \approx k_r^+ r\bar{p} - k_r^- r - r_g r, \tag{56}$$

$$\frac{dc}{dt} \approx (r_g - D)c, \tag{57}$$

where r_g is given by Eq. (47) and $\bar{x}, \bar{p}$ are given by Eq. (54).

The study of these dynamics is facilitated by observing that $\bar{p}$ is independent of the enzyme level (see (54)). Thus, we can study the slow motion during this phase by confining our attention to the two-dimensional system (56)–(57). At the heart of this simplification is that the fact that during this phase, the cells consume nearly all the substrate entering the chemostat. This ensures that the specific substrate uptake rate is effectively independent of the peripheral enzyme level ($r_s \approx Ds_f/c$). Now, the precursor levels sense the enzyme level through the specific substrate uptake rate (see (46)). Since the specific substrate uptake rate is independent of the enzyme level, so is $\bar{p}$. Thus, the ribosome level and cell density evolve without seeing the changes in the peripheral enzyme level.

Fig. 10b shows the motion of c and r on the phase plane. Note that

1. The phase path intersects both null-clines before reaching balanced growth. Hence, both c and r pass through extrema as they approach the steady state. Here also, the steady state is a stable focus since the eigenvalues of the linearization about the steady state are $\lambda_{1,2} = -0.2 \pm 0.1\imath$.
2. When the phase path crosses the null-cline for c, the sign of $\dot{c}$ changes from positive to negative. When it crosses the null-cline for r, the sign of $\dot{r}$ changes from negative to positive. This implies that c passes through a maximum while r passes through a minimum.
3. The phase path intersects the null-cline for c before it intersects the null-cline for r. It follows that c reaches its maximum before r attains its minimum.

These dynamics reflect that fact that the specific ribosome synthesis rate decreases first, followed by the specific protein synthesis and growth rates. Thus, at the beginning of Phase 4, $\dot{r} < 0$ because the synthesis rate of ribosomes has decreased much more than their dilution rate, and $\dot{c} > 0$ because of the inertia in the specific growth rate. As r decreases, so does the specific growth rate until it becomes equal to $D = 0.2\,1/h$. This is the point at which the cell density displays a maximum. As the ribosome levels, and hence, the specific growth rate, decrease further, the dilution rate of the ribosomes progressively decreases until their synthesis and dilution rates become equal. This is the point at which the ribosomes display a minimum.

We shall refer to these transients as *cell-sufficient fed-batch dynamics* because the fundamental property underlying these dynamics—the complete consumption of all the influent substrate ($Ds_f \approx r_s c$)—is characteristic of high-density fed-batch cultures.

3.2.3. Dilution rate shift-down

Fig. 11 shows the dynamics of a dilution rate shift-down. We assume that the initial dilution rate is close to the washout dilution rate, but not too close to it, so that the initial substrate concentration satisfies the inequality $K_s \ll s_0 \ll s_f$. The first inequality, $s_0 \gg K_s$, implies that the initial substrate concentration is at supersaturating levels. Consequently, there is an initial phase during which the cells continue to consume substrate and grow at their pre-shift rates, $r_{s,0}$ and D_0. The evolution of the substrate concentration and cell density during this initial growth phase is approximated by

$$\frac{ds}{dt} \approx D(s_f - s) - r_{s,0}c,$$

$$\frac{dc}{dt} \approx (D_0 - D)c.$$

Since $r_{s,0}c_0 = D_0(s_f - s_0)$, these equations imply that

$$s(t) \approx s_f - (s_f - s_0)\exp(D_0 - D)t, \tag{58}$$

$$c(t) \approx c_0 \exp(D_0 - D)t. \tag{59}$$

The second inequality, $s_0 \ll s_f$, implies that the initial cell density, $c_0 \approx \hat{Y}(s_f - s_0) \approx \hat{Y}s_f$, is large compared to the initial substrate concentration. The initial growth phase should, therefore, last for a relatively short period of time. This is indeed the case. To see this, observe that the initial exponential growth phase persists until the

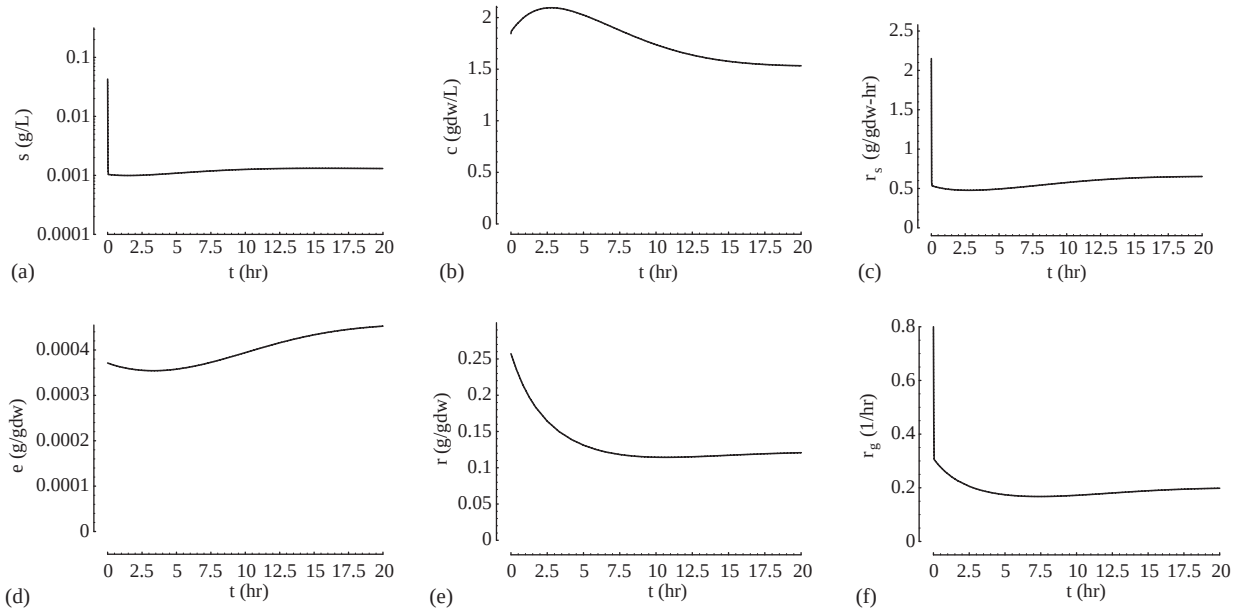

Fig. 11. Transient response to a dilution rate shift-down. At $t<0$, the culture is at the steady state corresponding to the dilution rate, $D_0 = 0.8\,1/h$, and feed concentration, $s_f = 5$ g/L. At $t = 0$, the dilution rate is shifted down to $D = 0.2\,1/h$, while the feed concentration is held constant.

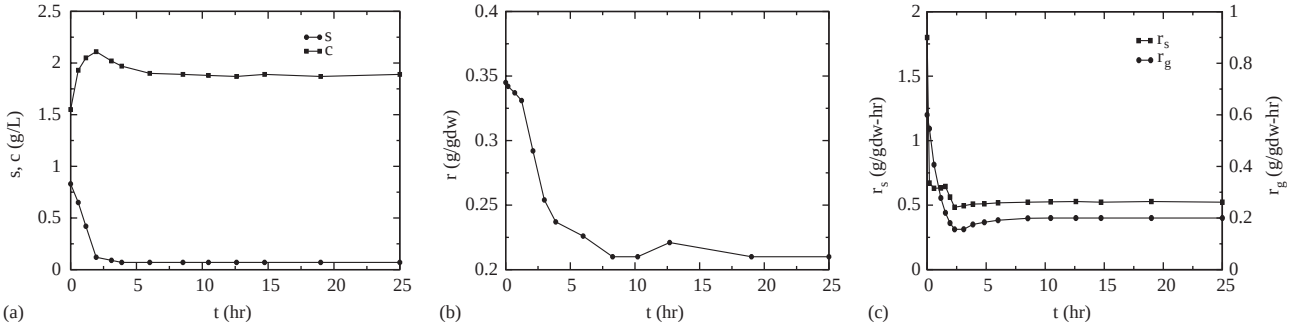

Fig. 12. Response of a glucose-limited culture of *E. coli* K12 to a dilution rate shift-down (from Yun et al., 1996). At $t<0$, the culture is at the steady state corresponding to the dilution rate, $D_0 = 0.6\,1/h$, and feed concentration, $s_f = 5\,g/L$. At $t = 0$, the dilution rate is shifted down to $D = 0.2\,1/h$, while the feed concentration is held constant. The figures show the evolution of the (a) Cell density and substrate concentration (b) RNA level (c) Specific substrate uptake growth rates calculated from the curves in (a).

substrate concentration drops to levels comparable to the saturation constant ($s \sim K_s$). It follows from Eq. (58) that the time taken to reach subsaturating substrate concentrations is given by the expression

$$\frac{1}{D_0 - D} \ln\left(\frac{1 - K_s/s_f}{1 - s_0/s_f}\right) \approx \frac{(s_0 - K_s)/s_f}{(D_0 - D)} \tag{60}$$

which is $\sim 0.2\,h$ if $s_0/s_f = 0.1$ and $D_0 - D = 0.5\,1/h$.

Once the substrate concentration reaches levels on the order of K_s, the reactor replicates the dynamics of phases 3 and 4 above. The cell density, the peripheral enzyme level and the ribosome concentration evolve slowly from the values achieved at the end of balanced growth to their ultimate steady-state values, while the substrate, inducer, and precursor levels remain at the quasisteady state concentrations defined by Eqs. (53) and (54).

The simulations are in good agreement with the data shown in Fig. 12, the only difference being that the predicted time interval of the initial exponential growth phase is smaller than the observed time interval of this phase. This is because in this experimental system, the initial substrate concentration and the saturation constant are relatively large ($s_0 \approx 1\,g/L$, $K_s = 0.1\,g/L$). The large initial substrate concentration increases the duration of the initial exponential growth phase (see (60)). The high saturation constant increases the time required for the substrate to switch from supersaturating to subsaturating levels.

3.2.4. Dilution rate shift-up

The response to dilution rate shift-ups also replicates the dynamics observed in feed switches. Fig. 13 shows the simulations of three dilution rate shift-ups from

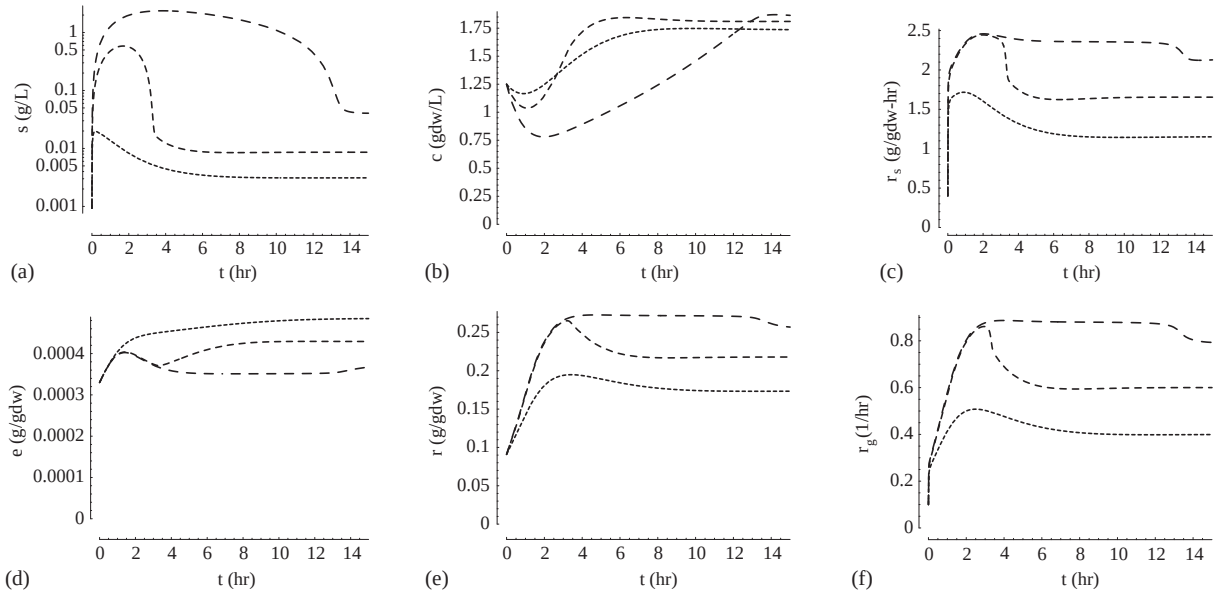

Fig. 13. Transient response to dilution rate shift-ups. At $t<0$, the culture is at the steady state corresponding to the dilution rate, $D_0 = 0.1\,1/h$, and feed concentration, $s_f = 5\,g/L$. At $t = 0$, the dilution rate is shifted up to $D = 0.4\,1/h$ (- -), $D = 0.6\,1/h$ (– –), and $D = 0.8\,1/h$ (— —).

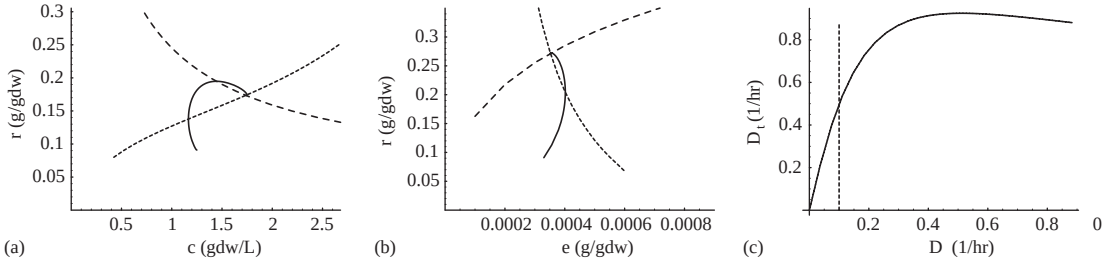

Fig. 14. Phase portraits of the slow motion during dilution rate shifts. (a) The slow motion corresponding to the dilution rate shift-up from $D_0 = 0.1\,1/h$ to $D = 0.4\,1/h$. The line with short dashes shows the null-cline for c; the line with long dashes shows the null-cline for r; the intersection of the two null-clines represents the steady-state concentrations of c and r at $D = 0.4\,1/h$; and the full line shows the motion of c and r from balanced growth toward the final steady state. (b) The slow motion corresponding to the large dilution rate shift-up from $D_0 = 0.1\,1/h$ to $D = 0.8\,1/h$. The line with short dashes shows the null-cline for e; the line with long dashes shows the null-cline for r; the intersection of the two null-clines represents the concentration of e and r at balanced growth; the full line shows the approach of e and r toward the state of balanced growth. (c) Classification of dilution rate shift-up dynamics.

$D_0 = 0.1\,1/h$ to $D = 0.4$, 0.6 and $0.8\,1/h$, respectively. In all three cases, the substrate concentration, the specific substrate uptake, and the specific growth rate rapidly increase within 10–15 min (Figs. 13a,c,f). However, the subsequent behavior of the three transients is quite different.

If the shift-up is small ($D = 0.4\,1/h$), the substrate concentration never achieves supersaturating concentrations. This is because the shift-up is so small that the rapid increment of the specific substrate uptake rate is sufficient to match the increase in the substrate input rate, Ds_f. Thus, within 10–15 min, the substrate reaches the quasisteady state concentration given by Eq. (53). The subsequent evolution is given by Eqs. (42)–(44), while,while s, x and p, are in the quasisteady states given by Eqs. (53) and (54), respectively. The phase portrait for this motion is shown in Fig. 14a.

If the shift-up is large ($D = 0.8\,1/h$), the substrate concentration rapidly reaches supersaturating levels, and remains at these levels throughout the subsequent transient. In this case, the shift-up is so large that the substrate uptake rate, $\bar{r}_s c_0$, cannot match the substrate input, Ds_f, even when the substrate concentration has reached supersaturating levels. Thus, the substrate concentration continues to increase, and remains at supersaturating levels. The rapid attainment of supersaturating substrate concentrations also stimulates the specific growth rate. As expected from the earlier analysis of continuous-to-batch shifts (Fig. 8), the specific growth immediately increases to $0.3\,1/h$ (Fig. 14f). But this enhanced specific growth rate falls well below the new dilution rate ($D = 0.8\,1/h$). Thus, in addition to accumulation of the substrate, there is a pronounced decline in the cell density which continues

until the ribosome levels have been built up to sufficiently high levels. These dynamics are similar to the Phases 1 and 2 dynamics of the feed switch. The phase portrait for this evolution is shown in Fig. 14b.

If the shift-up is intermediate ($D = 0.6\,1/h$), the substrate concentration saturates, and the physiological variables begin their approach to balanced growth, i.e., the cells go through Phase 1 and enter Phase 2. But before balanced growth is reached, the substrate concentration returns to subsaturating levels, and the cells switch to Phase 3 and 4 dynamics. Similar transients have been observed in experiments. Fig. 15 shows the response of a glycerol-limited culture of *K. aerogenes* to a dilution rate shift-up from $D_0 = 0.004\,1/h$ to $D = 0.24\,1/h$. The ribosome level, the specific growth rate, and the specific substrate uptake rate increase in a manner consistent with the approach to balanced growth (Figs. 15b,c). However, balanced growth is not fully attained because the substrate concentration drops to subsaturating levels well before the cells achieve balanced growth. Indeed, the substrate concentration drops to subsaturating levels at $t \approx 10\,h$ (Fig. 15a). At this point, the specific growth rate is $\sim 0.6\,1/h$, which is less than the maximum specific growth rate of $0.8\,1/h$.

Intuition suggests that the magnitude of the dilution rate shift-up required to provoke these dynamics depends on the initial dilution rate. For, if the initial dilution rate is very small, so is the initial enzyme level. In this case, relatively small shift-ups should yield supersaturating substrate concentrations, resulting in Phase 1 and 2 dynamics. On the other hand, if the initial dilution rate is large, the peripheral levels are so high that the substrate concentration should remain subsaturating throughout the transient, leading to Phase 3 and 4 dynamics. This is indeed the case. In fact, given the response to continuous-to-batch shifts (Fig. 4), one can predict the class of dynamics corresponding to any pre-assigned initial and final dilution rates. To see this, observe that the substrate concentration attains the quasisteady state given by Eq. (53) if and only if $\bar{r}_s(D_0)c_0 > Ds_f$, where $\bar{r}_s(D_0)$ denotes the specific substrate uptake rate achieved immediately after the cells have been exposed to supersaturating concentrations (see Fig. 8a). But it follows from Eq. (19) that $c_0 \approx D_0 s_f/\tilde{r}_s(D_0)$ at all but the highest dilution rates. We conclude that s attains quasisteady state if and only if

$$\bar{r}_s \frac{D_0 s_f}{\tilde{r}_s(D_0)} > Ds_f \quad \Rightarrow \quad D < D_0 \frac{\bar{r}_s(D_0)}{\tilde{r}_s(D_0)}.$$

In words, the substrate concentration attains quasisteady state if and only if the ratio by which the dilution rate increases, D/D_0, is less than ratio by which the specific uptake rate increases in response to a continuous-to-batch transition, $\bar{r}_s(D_0)/\tilde{r}_s(D_0)$. Thus, we can classify the dynamics by plotting the *transition* dilution rate

$$D_t \equiv D_0 \frac{\bar{r}_s(D_0)}{\tilde{r}_s(D_0)}$$

as a function of the initial dilution rate, D_0 (Fig. 14c). Given any D_0, Phase 1 and 2 dynamics are obtained if D lies above the curve; Phase 3 and 4 dynamics are obtained if D lies below the curve. In particular, one can see that the simulations shown in Fig. 13 are consistent with this classification.

4. Discussion

Chemostat dynamics have been the subject of numerous experimental studies. From this formidable body of literature, Daigger and Grady (1982) and Duboc et al. (1998) have distilled the key generalizations. We begin by reiterating these generalizations and interpreting them in terms of our model.

Based on an extensive review of the literature prior to 1980, Daigger and Grady classified the transients into two categories: growth responses and storage responses. Since our model does not account for storage, we

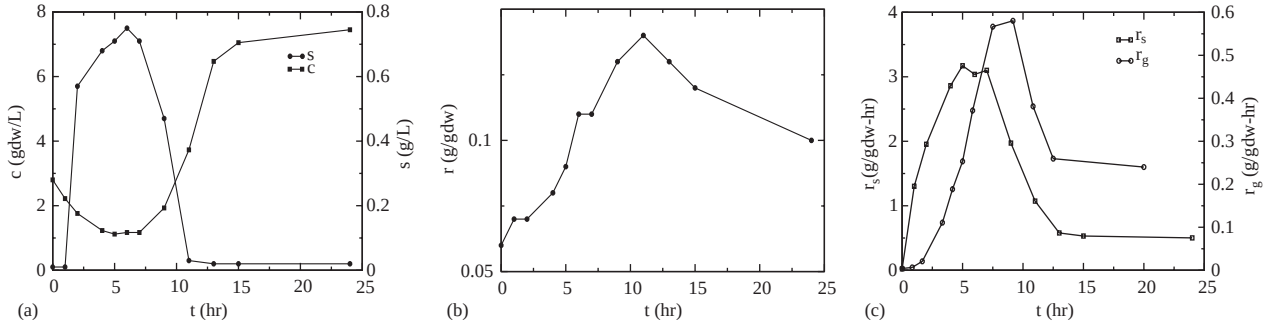

Fig. 15. Response of a glycerol-limited culture of *K. aerogenes* to a dilution rate shift-up (from Tempest et al., 1967). At $t<0$, the culture is at the steady state corresponding to the dilution rate, $D_0 = 0.004\,1/h$, and feed concentration, $s_f = 15\,g/L$. At $t = 0$, the dilution rate is shifted up to $D = 0.24\,1/h$, while the feed concentration is held constant. The figures show the evolution of the (a) Cell density and substrate concentration (b) RNA level (c) Specific substrate uptake and growth rates calculated from the curves in (a).

confine attention to the growth responses. They state that

1. The growth responses possess the following properties:
   (a) *Growth rate hysteresis* (*GRH*): During periods of varying substrate concentration, the specific growth rate of the culture lags behind the value predicted by the steady-state specific growth rate. During periods of decreasing concentration, the specific growth rate will be higher than predicted, while during periods of increasing substrate concentration, it will be lower than predicted.
   The model exhibits growth rate hysteresis. Indeed, Fig. 11f shows that immediately after the dilution rate shift-down, the culture settles into a specific growth rate that is higher than its final value. Conversely, the specific growth rate immediately after a dilution rate shift-up is lower than its ultimate value (Fig. 13f).
   (b) *Available growth potential* (*AGP*): Microbial cultures possess the ability to rapidly increase their growth and substrate uptake rates during a transient response. As a general rule, the degree to which a culture can immediately increase its growth and substrate removal rates increases as the steady state specific growth rate of the culture is decreased.
   Simulations of the continuous-to-batch shifts show that the specific substrate uptake and growth rates do increase immediately (Figs. 8a,c). Moreover, the increments in these rates increase as the dilution rate of the culture decreases. But this is true only up to a point. At sufficiently low dilution rates, the increments decrease once again because at very low dilution rates, the peripheral enzyme and ribosome levels become small.
2. In many instances, both phenomena are observed. For example, the specific growth rate immediately after exposure to substrate-excess conditions is greater than the rate before (AGP), but less than the maximum rate which the culture could attain. However, with the passage of time, the specific growth rate gradually increases, and eventually reaches the maximum rate. Throughout this period, the specific growth rate is less than the maximum specific growth rate (GRH).
   This property is evident in Figs. 9f and 13f.
3. The concept of physiological adaptation may be used to understand these growth responses. When a microbial culture is grown at a submaximal specific growth rate, the culture adapts to that growth environment. In particular, the RNA content, the enzyme levels, and concentration of intracellular metabolites are lower than the values attained at the maximum specific growth rate. When the cells are exposed to a substrate-excess environment, the culture is unable to grow at its maximum rate. This is because the physiological adaptation is not complete, so that the culture possesses only a limited ability to immediately increase its specific growth rate (AGP). As time passes, the levels of RNA, enzymes, and intracellular metabolites gradually increase. Thus, the specific growth rate of the culture increases progressively until it eventually reaches its maximum value (GRH).
   This train of events is precisely what transpires in the model (see Figs. 9 and 13).

More recently, Duboc et al. arrived at the following conclusions based on extensive dilution rate shift-up experiments with *S. cerevisiae* (Duboc et al., 1998).

1. There is an immediate increase in the catabolic activity. Moreover, the increase in the catabolic activity is always larger than the increase in the growth rate, leading to a transient uncoupling of catabolism and growth.
   This model displays this characteristic as is evident from Figs. 8a,c,d. To capture the different response times of the catabolic and anabolic rates, Duboc et al. assumed that these rates followed the phenomenological equations
   $$\tau_{cat}\frac{dr_{cat}}{dt} = (r_{cat}^{max} - r_{cat}), \quad \tau_g \frac{dr_g}{dt} = (r_g^{max} - r_g)$$
   and unique time constants, τ_{cat} and τ_g were chosen for each experiment in order to fit the data. Our model may be viewed as an attempt to give a physiological basis for the foregoing phenomenological equations.
2. In some experiments, such as the dilution rate shift-up of aerobic cultures limited by acetic acid, the transient behavior of the culture is similar to the adaptation of the metabolism during a batch experiment where substrate is in large excess and does not influence the specific growth rate. In yet other experiments, such as the dilution rate shift-up of glucose-limited aerobic cultures, the substrate did not accumulate.
   According to our model, these two transients reflect Phase 1/Phase 2 and Phase 3/Phase 4 dynamics, respectively. Since the maximum specific growth rate on acetic acid is much lower than the maximum specific growth rate on glucose, the very same dilution rate shift-up, i.e., the very same D_0 and D, could lead to substrate-sufficient batch dynamics in the first case, and cell-sufficient fed-batch dynamics in the second case.

The model yields further insights into these observations.

1. The substrate concentration exists in either one of two states. It is either at supersaturating levels or at the subsaturating levels attained when the substrate reaches quasisteady state. Transitions between these two states are so fast (on the order of minutes) that they may be ignored on the time-scale of interest (on the order of hours).
2. The dynamics corresponding to these two states are canonical in the following sense. The transients observed in response to a wide variety of perturbations are a combination of these two classes of dynamics. Thus, in dilution rate shift-ups, the substrate is supersaturating throughout the transient if the final dilution rate is close to the maximum specific growth rate. It is subsaturating throughout the transient if the final dilution rate is close to the initial dilution rate. It switches from supersaturating to subsaturating levels when the shift-ups are moderate. The latter is also the case in feed switches where the substrate concentration is supersaturating at first, but switches to subsaturating concentrations later. It follows that a complete understanding of these two classes of dynamics is sufficient for understanding all other dynamics.
3. These two classes of dynamics possess the following experimentally testable properties:
   (a) During the approach to balanced growth, the peripheral enzyme and ribosome levels pass through a maximum, but the enzyme level reaches a maximum before the ribosome level.
   (b) During the approach to the final steady state, the cell density passes through a maximum and the ribosome level passes through a minimum. The cell density reaches its maximum before the ribosome level reaches its minimum.

We can express these observations more concisely in the parlance of nonlinear dynamics. We have shown, in effect, that the chemostat displays *excitable* dynamics. In other words, there are two "slow" submanifolds (surfaces) embedded within the space of all variables in the model. The motion into and out of these submanifolds is very fast. The dynamics on the time-scale of interest (h) occur only when the variables lie in one of the submanifolds. The motion on these two submanifolds corresponds to Phase 1/Phase 2 and Phase 3/Phase 4 dynamics, respectively.

We note finally that the model does not account for certain features of microbial growth. As observed in Section 1

1. There is evidence indicating that biosynthesis is limited by GDH rather than ribosomes.
2. The excess substrate imported by the cell is eliminated by respiration, excretion and storage.

Extensions of the model accounting for the roles of GDH, excretion, and storage are currently under investigation.

5. Conclusions

We have formulated a model of microbial growth accounting for both inducible enzyme synthesis and ribosome-mediated protein synthesis. The fundamental assumption made was that synthesis of ribosomes is autocatalytic, an assumption based on the experimentally observed RNA synthesis rates. Both the steady states and the transients of the model show remarkable agreement with a wide variety of experimental data. Analysis of the model yields simple explanations of seemingly complex behavior.

1. Steady states
   (a) The cell density decreases at low dilution rates. This behavior does not stem from an ad hoc maintenance. It falls out naturally as a consequence of the futile cycling of RNA at low dilution rates.
   (b) The peripheral enzyme level passes through a maximum. This reflects the competing effects of enzyme induction and dilution. At low dilution rates, induction dominates, so that the peripheral enzyme level is an increasing function of D. At high dilution rates, dilution dominates, and the peripheral enzyme level is a decreasing function of D.
   (c) The ribosome levels approach a nonzero level at small dilution rates. According to the model, this is the result of the futile cycling of proteins.
   As the dilution rate increases, the ribosome levels increase monotonically. This is a consequence of the assumption that protein synthesis rate is proportional to the concentration of ribosomes. It provides a simple answer to the question of *growth rate control* (Roberts, 1997): Why does the steady-state ribosome level increase linearly with the dilution rate?
2 Transients
   (a) The model shows good agreement with a wide variety of transients including continuous-to batch shifts, feed switches, dilution rate shift-ups and dilution rate shift-downs.
   (b) We show that the bewildering array of transients observed are in fact combinations of two canonical dynamics, namely, the approach to balanced growth under supersaturating substrate concentrations, and the approach to steady state under subsaturating substrate concentrations. In dilution rate shifts, for instance, only one of these canonical dynamics occurs. In feed switches, the

two canonical dynamics occur sequentially. The cells begin by approaching balanced growth under supersaturating concentrations, and then move toward the final steady state under sub-saturating substrate concentrations.

The practical importance of this result is the following. To understand the dynamics of a chemostat, it suffices to confine attention to these two canonical dynamics. All other dynamics can be inferred from them.

(c) The particular class of canonical dynamics that will be observed in dilution rate shift-ups can be predicted from continuous-to-batch shift data.

Appendix A. Order-of-magnitude estimates of the parameter values

The orders of magnitude of the parameters for substrate uptake and peripheral enzyme synthesis are based on kinetic properties of the *lac* operon.

1. The maximum velocity of lactose transport is 60,000 molecules per minute per permease molecule (Chung and Stephanopoulos, 1996). Since the molecular weights of lactose and permease are 342 and 46,504 (Neidhardt et al., 1987, p. 1446), respectively

   $V_s \sim 10^4$ g/(g enzyme-h).

2. The saturation constant for lactose transport is 5×10^{-4} moles/l (Chung and Stephanopoulos, 1996)

   $K_s \sim 10^{-2}$ g/L.

3. The inducer concentration is 10^{-3} g/gdw (Chung and Stephanopoulos, 1996). Since $r_s \sim 1$ g/(gdw-h), Eq. (45) implies that

   $k_x \sim 10^3$ g/(g inducer-h).

4. The maximum velocity of permease synthesis is 10^{-8} mole/min^{-1} (Chung and Stephanopoulos, 1996). Since each liter of cell volume contains roughly 400 gdw

   $V_e \sim 10^{-4}$ g/(gdw-h).

5. Vogel and Jensen exposed exponentially growing cells growing at various specific growth rates to supersaturating concentrations of IPTG, a gratuitous inducer of the *lac* operon, and measured the specific β-galactosidase rate immediately after the exposure (Vogel and Jensen, 1994). They found that the instantaneous specific enzyme synthesis rate is an increasing function of the specific growth rate, and achieves half-saturation at $r_g \approx 0.1$ 1/h. Since $\tilde{r} \sim 0.1$ g/gdw at this dilution rate

   $K_e \sim 0.1$ g/gdw.

6. The equilibrium constant K_2 is 10^{11}(L/mol)^2 (Yagil and Yagil, 1971). Since the molecular weight of the repressor ($\sim 10^5$ g/mol) is much larger than the molecular weight of the inducer ($\sim 10^2$ g/mol)

   $K_2 \sim 10^{11}$(gdw/g)^2.

7. The enzyme degradation rate is on the order 0.01 1/h (Neidhardt et al., 1987, Chapter 44)

   $k_e^- \sim 10^{-2}$ 1/h.

8. At $D \approx 1$ 1/h, 90% of the rRNA synthesized is incorporated into biomass and the remaining 10% is degraded (Gausing, 1977), i.e.,[7]

   $$\frac{r_r^-}{r_g r} = \frac{k_r^-}{D} = \frac{1}{9} \Rightarrow k_r^- \approx 0.1\,1/\text{h}.$$

9. The precursor concentration is on the order of 0.01 g/gdw (Neidhardt et al., 1990); we assumed that

   $K_c, K_i \sim 0.001$ g/gdw.

10. The protein degradation rate is on the order of 0.01 1/h (Neidhardt et al., 1987, Chapter 44)

    $k_r^- \sim 0.01\,1/\text{h}$.

11. The specific protein synthesis rate is on the order of 0.1 g/(gdw-h). Since $r \sim 0.1$ g/gdw

    $V_c \sim 1$ g protein/(g RNA-h).

12. The specific rRNA synthesis rate is on the order of 0.1 g/(gdw-h) (Gausing, 1977). Since $r_r^+ = k_r^+ pr \sim 0.1$ g/gdw, $p \sim 0.01$ g/gdw, and $r \sim 0.1$ g/gdw

    $k_r^+ \sim 100$ gdw/(g-h).

13. According to the model, the maximum yield on biomass is $k_r^+/(k_r^+ + k_{co_2})$ (see (26)). Since the maximum yield for typical sugars is ~ 0.4 gdw/g, we assumed that

    $k_{co_2} \sim 150\,1/\text{h}$.

[7] At low dilution rates ($D \approx 0.007$ 1/h), the specific degradation rate is higher ($k_r^- \approx 0.16$ 1/h), since 30% of the rRNA synthesized is incorporated into biomass, and 70% is degraded. However, the order of magnitude remains unchanged.

Appendix B. Stability of the death steady states

The variational matrix W of Eqs. (34)–(39) is given by

$$W = \begin{pmatrix} \dfrac{\partial(\dot{s},\dot{c})}{\partial(s,c)} & 0 \\ * & \dfrac{\partial(\dot{c}^-,\dot{e},\dot{r},\dot{x})}{\partial(\dot{c}^-,\dot{e},\dot{r},\dot{x})} \end{pmatrix}, \tag{61}$$

where

$$\frac{\partial(\dot{s},\dot{c})}{\partial(s,c)} = \begin{pmatrix} -D & -r_s \\ 0 & r_g - D \end{pmatrix}.$$

Since the submatrix $\partial(\dot{s},\dot{c})/\partial(s,c)$ contributes two negative eigenvalues $-D$ and $r_g - D$, the stability of a death steady state is determined exclusively by the submatrix $J = \partial(\dot{c}^-,\dot{e},\dot{r},\dot{x})/\partial(c^-,e,r,x)$.

We begin by observing that Eq. (39) together with

$$r_s = \frac{V_s e s_f/(K_s + s_f)}{(1 + p/K_i)}, \quad r_g = r_s - k_{\mathrm{co}_2} p$$

imply that

$$\frac{\partial r_s}{\partial z} \geqslant 0, \quad \frac{\partial r_g}{\partial z} = \frac{\partial r_s}{\partial z} + k_{\mathrm{co}_2} > 0$$

for any choice of the physiological variable $z \in \{c^-, e, r, x\}$.

B.1. Stability of case A

In this case, $\tilde{r} = \tilde{e} = \tilde{x} = 0$, $\tilde{c}^-, \tilde{p} > 0$, and $\tilde{r}_g = -k_c^-$. The submatrix J is given by

$$J_A = \begin{pmatrix} -\frac{\partial r_g}{\partial c^-}\tilde{c}^- & -\frac{\partial r_g}{\partial e}\tilde{c}^- & V_c\frac{\tilde{p}}{K_c+\tilde{p}} - \frac{\partial r_g}{\partial r}\tilde{c}^- & \frac{\partial r_g}{\partial x}\tilde{c}^- \\ 0 & k_c^- - k_e^- & \rho'(0)R(0) & 0 \\ 0 & 0 & k_r^+\tilde{p} - k_r^- + k_c^- & 0 \\ 0 & \frac{\partial r_s}{\partial e} & 0 & k_c^- - k_x \end{pmatrix}, \tag{62}$$

where $\rho(r) \equiv V_e r/(K_e + r)$ and $R(x) \equiv (1 + K_1 x^2)/(K_3 + K_2 x^2)$. The eigenvalues of J_A are simply given by the diagonal entries. Since $-\frac{\partial r_g}{\partial c^-}\, c^- < 0$, the equilibrium of case A is stable if and only if

$$k_c^- < \min(k_e^-, k_x), \quad k_r^+ \frac{k_c^-}{k_{\mathrm{co}_2}} - k_r^- + k_c^- < 0.$$

B.2. Stability of case B

In this case, $\tilde{r} = \tilde{c}^- = 0$, $\tilde{e}, \tilde{x}, \tilde{p} > 0$, and $\tilde{r}_g = -k_e^-$. The submatrix J is given by

$$J_B = \begin{pmatrix} k_e^- - k_c^- & 0 & V_c\frac{\tilde{p}}{K_c+\tilde{p}} & 0 \\ -\frac{\partial r_g}{\partial c^-}\tilde{e} & -\frac{\partial r_g}{\partial e}\tilde{e} & \rho'(0)R(\tilde{x}) - \frac{\partial r_g}{\partial r}\tilde{e} & -\frac{\partial r_g}{\partial x}\tilde{e} \\ 0 & 0 & k_r^+\tilde{p} - k_r^- + k_e^- & 0 \\ \frac{\partial r_s}{\partial c^-} - \frac{\partial r_g}{\partial c^-}\tilde{x} & \frac{\partial r_s}{\partial e} - \frac{\partial r_g}{\partial e}\tilde{x} & \frac{\partial r_s}{\partial r} - \frac{\partial r_g}{\partial r}\tilde{x} & \frac{\partial r_s}{\partial x} - \frac{\partial r_g}{\partial x}\tilde{x} \end{pmatrix}. \tag{63}$$

Two eigenvalues of J_B are given by

$$k_e^- - k_c^- \quad \text{and} \quad k_r^+\tilde{p} - k_r^- + k_e^-$$

and the remaining two are determined by the submatrix

$$J'_B = \begin{pmatrix} -\dfrac{\partial r_g}{\partial e}\tilde{e} & -\dfrac{\partial r_g}{\partial x}\tilde{e} \\ \dfrac{\partial r_s}{\partial e} - \dfrac{\partial r_g}{\partial e}\tilde{x} & \dfrac{\partial r_s}{\partial x} - \dfrac{\partial r_g}{\partial x}\tilde{x} \end{pmatrix}.$$

In the remainder of this section, we show that the matrix J'_B is always stable, i.e. it contributes two negative eigenvalues. We begin by reiterating that

$$\frac{\partial r_g}{\partial e} = \frac{\partial r_s}{\partial e} + k_{\mathrm{co}_2} > 0, \quad \frac{\partial r_g}{\partial x} = \frac{\partial r_s}{\partial x} + k_{\mathrm{co}_2} > 0.$$

In addition, the functional form of r_s implies that

$$\frac{\partial r_s}{\partial e} = \frac{\partial r_s}{\partial x} + \frac{r_s}{\tilde{e}},$$

so that

$$\frac{\partial r_g}{\partial e} = \frac{\partial r_g}{\partial x} + \frac{r_s}{e}, \quad \frac{\partial r_g}{\partial e} - \frac{\partial r_g}{\partial x} > 0.$$

Taking these relations into account, the matrix J'_B can be equivalently written as

$$J'_B = \begin{pmatrix} -\dfrac{\partial r_g}{\partial e}\tilde{e} & -\dfrac{\partial r_g}{\partial x}\tilde{e} \\ \dfrac{\partial r_g}{\partial e}(1-\tilde{x}) - k_{\mathrm{co}_2} & \dfrac{\partial r_g}{\partial x}(1-\tilde{x}) - k_{\mathrm{co}_2} \end{pmatrix}.$$

The determinant of J'_B is given by

$$\det J'_B = \frac{\partial r_g}{\partial e} e\left(k_{\mathrm{co}_2} - \frac{\partial r_g}{\partial x}(1-x)\right) + \frac{\partial r_g}{\partial x} e\left(\frac{\partial r_g}{\partial e}(1-x) - k_{\mathrm{co}_2}\right),$$

which simplifies to

$$\det J'_B = \tilde{e} k_{\mathrm{co}_2}\left(\frac{\partial r_g}{\partial e} - \frac{\partial r_g}{\partial x}\right) > 0.$$

The trace of J'_B is given by

$$\mathrm{tr}\, J'_B = -\frac{\partial r_g}{\partial e}\tilde{e} + \frac{\partial r_g}{\partial x}(1-x) - k_{\mathrm{co}_2}.$$

Since $\frac{\partial r_g}{\partial e}e = r_s + \frac{\partial r_g}{\partial x}e$, and $e + x + p = 1$, we have that

$$\begin{aligned}\operatorname{tr} J'_B &= -r_s - k_{co_2} + \frac{\partial r_g}{\partial x}(1 - \tilde{x} - \tilde{e}) \\ &= -r_s - k_{co_2} + \frac{\partial r_g}{\partial x}\tilde{p}.\end{aligned}$$

Since in addition,

$$\frac{\partial r_g}{\partial x} = r_s \frac{\frac{1}{K_i}}{1 + \frac{\tilde{p}}{K_i}} + k_{co_2},$$

we finally obtain that

$$\operatorname{tr} J'_B = -r_s\left(1 - \frac{\frac{\tilde{p}}{K_i}}{1 + \frac{\tilde{p}}{K_i}}\right) - k_{co_2}(1 - \tilde{p}) < 0.$$

Since $\det J'_B > 0$ and $\operatorname{tr} J'_B < 0$, the matrix J'_B is a stability matrix.

To summarize, the equilibrium of case B is stable if and only if both inequalities

$$k_e^- - k_c^- < 0 \quad \text{and} \quad k_r^+\tilde{p} - k_r^- + k_e^- < 0$$

hold. Note that death states A and B cannot be stable simultaneously because the state A has the eigenvalue $k_c^- - k_e^-$ and the state B has the eigenvalue $k_e^- - k_c^-$. These quantities clearly have opposite signs.

B.3. Stability of case C

In this case, $\tilde{r} = \tilde{e} = \tilde{c}^- = 0$, $\tilde{x}, \tilde{p} > 0$, and $\tilde{r}_g = -k_x$. The submatrix J is given by

$$J_C = \begin{pmatrix} k_x - k_c^- & 0 & V_c\frac{\tilde{p}}{K_c + \tilde{p}} & 0 \\ 0 & k_x - k_e^- & \rho'(0)R(x) & 0 \\ 0 & 0 & k_r^+\tilde{p} - k_r^- + k_x & 0 \\ 0 & \frac{\partial r_s}{\partial e} - \frac{\partial r_g}{\partial e}\tilde{x} & -\frac{\partial r_g}{\partial r}\tilde{x} & -\frac{\partial r_g}{\partial x}\tilde{x} \end{pmatrix}. \tag{64}$$

Similar to case A, the eigenvalues of J_C are simply given by the diagonal entries. Since $-\frac{\partial r_g}{\partial x}x < 0$, the equilibrium of case C is stable if and only if

$$k_x < \min(k_c^-, k_e^-), \quad k_r^+\frac{k_x}{k_{co_2}} - k_r^- + k_x < 0.$$

B.4. Stability of case D

In this case, $\tilde{r} = \tilde{e} = \tilde{c}^- = \tilde{x} = 0$, $\tilde{p} = 1$, and $\tilde{r}_g = -k_{co_2}$.

The submatrix J is given by

$$J_D = \begin{pmatrix} k_{co_2} - k_c^- & 0 & V_c\frac{1}{K_c + 1} & 0 \\ 0 & k_{co_2} - k_e^- & \rho'(0)R(0) & 0 \\ 0 & 0 & k_{co_2} - k_r^- & 0 \\ 0 & \frac{\partial r_s}{\partial e} & 0 & k_{co_2} - k_x \end{pmatrix}. \tag{65}$$

Again, the eigenvalues of J_D are given by the diagonal entries. The equilibrium of case D is stable if and only if $k_{co_2} < \min(k_c^-, k_e^-, k_r^-, k_x)$.

Appendix C. Derivation of the reduced equations

If we define the dimensionless variables

$$\hat{s} \equiv \frac{s}{s_r}, \quad \hat{c} \equiv \frac{c}{s_r}, \quad \hat{x} \equiv \frac{x}{x_r},$$
$$\hat{e} \equiv \frac{e}{e_r}, \quad \hat{r} \equiv \frac{r}{r_r}, \quad \hat{p} \equiv \frac{p}{p_r},$$
$$\hat{c}^- \equiv \frac{c^-}{c_r^-}\ \hat{t} \equiv \frac{t}{t_r},$$

where

$$s_r = s_f, \quad c_r = s_f, \quad x_r = \sqrt{\frac{V_s V_e}{k_x}},$$
$$e_r = \sqrt{\frac{V_e}{V_s}}, \quad r_r = \frac{\sqrt{V_s V_e}}{V_c}, \quad p_r = \frac{\sqrt{V_s V_e}}{k_{co_2}},$$
$$c_r^- = 1, \quad t_r = \frac{1}{\sqrt{V_s V_e}}$$

we obtain the dimensionless equations

$$\frac{d\hat{s}}{d\hat{t}} = \hat{D}(1 - \hat{s}) - \hat{r}_s\hat{c}, \tag{66}$$

$$\frac{d\hat{c}}{d\hat{t}} = (\hat{r}_g - \hat{D})\hat{c}, \tag{67}$$

$$\frac{d\hat{e}}{d\hat{t}} = \hat{r}_e^+ - \hat{r}_e^- - \hat{r}_g\hat{e}, \tag{68}$$

$$\frac{d\hat{r}}{d\hat{t}} = \hat{r}_r^+ - \hat{r}_r^- - \hat{r}_g\hat{r}, \tag{69}$$

$$\tau_x\frac{d\hat{x}}{d\hat{t}} = \hat{r}_s - \hat{r}_x - \tau_x\hat{r}_g\hat{x}, \tag{70}$$

$$\begin{aligned}\tau_p\frac{d\hat{p}}{d\hat{t}} = {} & \hat{r}_x - \hat{r}_{co_2} - (\hat{r}_c^+ - \hat{r}_c^-) - r_r(\hat{r}_r^+ - \hat{r}_r^-) \\ & - e_r(\hat{r}_e^+ - \hat{r}_e^-) - \tau_p\hat{r}_g\hat{p},\end{aligned} \tag{71}$$

$$\hat{c}^- = 1 - r_r\hat{r} - e_r\hat{e} - x_r\hat{x} - p_r\hat{p}, \tag{72}$$

with dimensionless rates

$$\hat{r}_s \equiv \hat{e}\,\frac{\hat{s}}{\hat{K}_s+\hat{s}}\,\frac{1}{1+\hat{p}/\hat{K}_i},\quad \hat{r}_e^+ \equiv \frac{\hat{r}}{\hat{K}_e+\hat{r}}\,\frac{1+\hat{K}_2\hat{x}^2}{K_3+\hat{K}_2\hat{x}^2},$$
$$\hat{r}_e^- = \hat{k}_e^-\hat{e},\quad \hat{r}_r^+ \equiv \hat{k}_r^+\hat{p}\hat{r},\quad \hat{r}_r^- = \hat{k}_r^-\hat{r},$$
$$\hat{r}_x \equiv \hat{x},\quad \hat{r}_{co_2} \equiv \hat{p},\quad \hat{r}_c^+ \equiv \hat{r}\,\frac{\hat{p}}{\hat{K}_c+\hat{p}},$$
$$\hat{r}_c^- \equiv \hat{k}_c^-\hat{c}^-,\quad \hat{r}_g \equiv \hat{r}_s - \hat{r}_{co_2}$$

and dimensionless parameters

$$\hat{D} \equiv Dt_r,\quad \hat{K}_s \equiv \frac{K_s}{s_r},\quad \hat{K}_i \equiv \frac{K_i}{p_r},\quad \hat{K}_e \equiv \frac{K_e}{r_r},$$
$$\hat{K}_2 \equiv K_2x_r^2,\quad \hat{k}_e^- \equiv k_e^-t_r,$$
$$\hat{k}_r^+ \equiv \frac{k_r^+}{k_{co_2}},\quad \hat{k}_r^- \equiv k_r^-t_r,\quad \tau_x \equiv \frac{1}{k_xt_r},\quad \tau_p \equiv \frac{1}{k_{co_2}t_r},$$
$$\hat{K}_c \equiv \frac{K_c}{p_r},\quad \hat{k}_c^- \equiv k_c^-t_r.$$

Since $\tau_x, \tau_p, e_r, x_r, p_r \ll 1$, Eqs. (70)–(72) become

$$0 \approx \hat{r}_s - \hat{r}_x,$$

$$0 \approx \hat{r}_x - \hat{r}_{co_2} - (\hat{r}_c^+ - \hat{r}_c^-) - r_r(\hat{r}_r^+ - \hat{r}_r^-),$$

$$1 \approx \hat{c}^- + r_r r.$$

It follows from the first two equations that

$$\hat{r}_g \equiv \hat{r}_s - \hat{r}_{co_2} \approx (\hat{r}_c^+ - \hat{r}_c^-) + r_r(\hat{r}_r^+ - \hat{r}_r^-).$$

In other words, X and P rapidly achieve quasisteady state, and the specific growth rate during the subsequent motion is effectively the sum of the net specific protein and RNA synthesis rates. Thus, we arrive at the equations

$$\frac{d\hat{s}}{d\hat{t}} = \hat{D}(1-\hat{s}) - \hat{r}_s\hat{c},$$

$$\frac{d\hat{c}}{d\hat{t}} = (\hat{r}_g - \hat{D})\hat{c},$$

$$\frac{d\hat{e}}{d\hat{t}} = \hat{r}_e^+ - \hat{r}_e^- - \hat{r}_g\hat{e},$$

$$\frac{d\hat{r}}{d\hat{t}} = \hat{r}_r^+ - \hat{r}_r^- - \hat{r}_g\hat{r},$$

$$0 \approx \hat{r}_s - \hat{r}_x,$$

$$0 \approx \hat{r}_x - \hat{r}_{co_2} - r_g,$$

$$\hat{c}^- \approx 1 - r_r\hat{r}.$$

The reduced equations are obtained from these equations by reverting to the original (dimensional) variables.

The approximate "slow" manifold is unique and globally stable. To see this, consider the approximate "fast" equations

$$\dot{x} = \frac{V_s e\ \sigma(s)}{1+\frac{p}{K_i}} - k_x x, \tag{73}$$

$$\dot{p} = k_x x - k_{co_2}p - V_c r\frac{p}{K_c+p} - k_r^+ rp + k_r^- r + k_c^- c^- \tag{74}$$

and assuming that the slow variables s, e, r, $c^- > 0$ are constant, we can show the following:

1. If $x = 0$ and $p \geqslant 0$ then $\dot{x} > 0$ due to Eq. (73). If $p = 0$ and $x \geqslant 0$ then $\dot{p} > 0$ due to Eq. (74). Hence both x and p remain strictly positive at all times.
2. If $p \geqslant 0$ and x becomes too large, namely if $x > \frac{V_s e\sigma}{k_x}$, then $\dot{x} < 0$ due to Eq. (73). Hence x remains bounded at all times. Since x remains bounded, Eq. (74) implies that p also remains bounded.
3. For any combination s, e, r, $c^- > 0$, the Jacobian of Eqs. (73)–(74) has the form
$$J = \frac{\partial(\dot{x},\dot{p})}{\partial(x,p)} = \begin{pmatrix} - & - \\ + & - \end{pmatrix}. \tag{75}$$
This implies several things:
   (a) Since the divergence of Eqs. (73)–(74) (equivalently, the trace of J) is negative for all x, $p \geqslant 0$, the system (73)–(74) cannot have periodic solutions. Since all positive solutions are bounded, every positive solution must converge to a steady state. In addition, the signs of the off-diagonal entries of J are such that the orbits in the (x,p) plane rotate counterclockwise.
   (b) At any steady state of Eqs. (73)–(74), we have that $\operatorname{tr} J < 0$ and $\det J > 0$. Thus all steady states must be stable. Therefore, only one positive steady state of Eqs. (73)–(74) must exist.

We conclude that for any combination s, e, r, $c^- > 0$, the fast system (73)–(74) admits a unique globally stable quasisteady state $(\overline{x}, \overline{p})$. Hence, the QSSA is well defined for all s, e, r, $c^- > 0$.

References

Bally, M., Egli, T., 1996. Dynamics of substrate consumption and enzyme synthesis in *Chelatobacter heintzii* during growth in carbon-limited continuous culture with different mixtures of glucose and nitrilotriacetic acid (NTA). Appl. Environ. Microbiol. 62, 133–140.

Baloo, S., Ramkrishna, D., 1990. Metabolic regulation in bacterial continuous cultures—I. Biotechnol. Bioeng. 29, 940–943.

Bremer, H., 1975. Parameters affecting the rate of synthesis of ribosomes and RNA polymerase in bacteria. J. Theor. Biol. 53, 115–124.

Bremer, H., Dennis, P.P., 1975. Transition period following a nutritional shift-up in the bacterium *Escherichia coli* B/r: Stable RNA and protein synthesis. J. Theor. Biol. 52, 365–382.

Brunschede, H., Dove, T.L., Bremer, H., 1977. Establishment of exponential growth after a nutritional shift-up in *Escherichia coli*

B/r: Accumulation of deoxyribonucleic acid, ribonucleic acid, and protein. J. Bacteriol. 129, 1020–1033.
Chung, J.D., Stephanopoulos, G., 1996. On physiological multiplicity and population heterogeneity of biological systems. Chem. Eng. Sci. 51, 1509–1521.
Cooney, C.L., Wang, D.I.C., Mateles, R.I., 1976. Growth of *Enterobacter aerogenes* in a chemostat with double nutrient limitations. Appl. Environ. Microbiol. 31, 91–98.
Daigger, G.T., Grady Jr., C.P.L., 1982. The dynamics of microbial growth on soluble substrates. Biotechnol. Bioeng. 16, 365–382.
Davis, B.D., Luger, S.M., Tai, P.C., 1986. Role of ribosome degradation in the death of starved *Escherichia coli* cells. J. Bacteriol. 166, 439–445.
Domach, M.M., Leung, S.K., Cahn, R.E., Cocks, G.G., Shuler, M.L., 1984. Computer model for glucose-limited growth of a single cell of *escherichia coli* B/r-A. Biotechnol. Bioeng. 26, 203–216.
Duboc, p., von Stockar, U., Villadsen, J., 1998. Simple generic model for dynamic experiments with *Saccharomyces cerevisiae* in continuous culture: Decoupling between anabolism and catabolism. Biotechnol. Bioeng. 60, 180–189.
Egli, T., 1995. The ecological and physiological significance of the growth of heterotrophic microorganisms with mixtures of substrates. Adv. Microbiol. Ecol. 14, 305–386.
Gaal, T., Bartless, M.S., Ross, W., Turnbough Jr., C.L., Gourse, R.L., 1997. Transcription regulation by initiating NTP concentration: rRNA synthesis in bacteria. Science 278, 2092–2097.
Gausing, K., 1977. Regulation of ribosome production in *Escherichia coli*: Synthesis and stability of ribosomal RNA and of ribosomal protein messenger RNA at different growth rates. J. Mol. Biol. 115, 335–354.
Grady Jr., C.P.L., Harlow, L.J., Riesing, R.R., 1972. Effects of growth rate and influent substrate concentrations on effluent quality from chemostats containing bacteria in pure and mixed culture. Biotechnol. Bioeng. 14, 391–410.
Harvey, R.J., 1970. Metabolic regulation in glucose-limited chemostat cultures of *Escherichia coli*. J. Bacteriol. 104, 698–706.
Hunter, I.S., Kornberg, H.L., 1979. Glucose transport of *Escherichia coli* growing in a glucose-limited continuous culture. Biochem. J. 178, 97–101.
Jensen, K.F., Pedersen, S., 1990. Metabolic growth rate control in *Escherichia coli* may be a consequence of subsaturation of the macromolecular biosynthetic apparatus with substrates and catalytic components. Microbiol. Rev. 54, 89–100.
Kaplan, R., Apirion, D., 1975. The fate of ribosomes in *Escherichia coli* cells starved for a carbon source. J. Biol. Chem. 250, 1854–1863.
Koch, A.L., 1970. Overall controls on the biosynthesis of ribosomes in growing bacteria. J. Theor. Biol. 28, 203–231.
Lin, E.C.C., 1987. Dissimilatory pathways for sugars, polyols, and carboxylates. In: Neidhardt, F.C., Ingraham, J.L., Schaechter, M., Brooks, K., Magasanik, B., Umbarger, H.E. (Eds.), *Escherichia coli* and *Salmonella typhimurium*: Cellular and Molecular Biology, vol. 1. American Society for Microbiology, Washington DC, pp. 244–284 (Chapter 18).
Maaloe, O., Kjeldgaard, N.O., 1966. Control of macromolecular synthesis: A study of DNA, RNA, and protein synthesis. In: Microbial and Molecular Biology. W. A. Benjamin, New York.
Nagai, S., Nishizawa, Y., Endo, I., Aiba, S., 1968. Response of a chemostatic culture of *Azotobacter vinelandii* to a delta type pulse of glucose. J. Gen. Appl. Microbiol. 14, 121–134.
Neidhardt, F.C., Ingraham, J.L., Schaechter, M., Brooks, K., Magasanik, B., Umbarger, H.E. (Eds.), 1987. *Escherichia coli* and *Salmonella typhimurium*: Cellular and Molecular Biology, vol. 2. American Society for Microbiology, Washington DC.
Neidhardt, F.C., Ingraham, J.L., Schaechter, M., 1990. Physiology of the Bacterial Cell: A Molecular Approach. Frank Sinauer Associates, Sunderland, MA.
Neijssel, O.M., Hueting, S., Tempest, D.W., 1977. Glucose transport capacity is not the rate-limiting step in the growth of some wild-type strains of *Escherichia coli* and *Klebsiella aerogenes* in chemostat culture. FEMS Microbiol. Lett. 2, 1–3.
Nielsen, J., Villadsen, J., 1992. Modeling of microbial kinetics. Chem. Eng. Sci. 47, 4225–4270.
Nomura, M., 1984. The control of ribosome synthesis. Sci. Am. 250, 102–114.
O'Brien, R.W., Neijssel, O.M., Tempest, D.W., 1980. Glucose phosphoenolpyruvate phosphotransferase activity and glucose uptake rate of *Klebsiella aerogenes* growing in a chemostat culture. J. Gen. Microbiol. 116, 305–314.
Petersen, C., Moller, L.B., 2000. Invariance of the nucleoside triphosphate pools of *Escherichia coli* with growth rate. J. Biol. Chem. 275, 3931–3935.
Plumbridge, J., 2003. Regulation of gene expression in the PTS in *Escherichia coli*: The role and interactions of Mlc. Curr. Opin. Microbiol. 5, 187–193.
Powell, E.O., 1969. Transient changes in the growth rate of microorganisms. In: Malek, I., Bevan, K., Fencl, Z., Munk, V., Ricica, J., Smrckova, H. (Eds.), Continuous Cultivation of Microorganisms. Academic Press, New York, pp. 275–284.
Ramkrishna, D., 2003. On modeling of bioreactors for control. J. Proc. Control 13, 581–589.
Reitzer, L.J., Magasanik, B., 1987. Ammonia assimilation and the biosynthesis of glutamine, glutamate, aspartate, asparagine, L-alanine, and D-alanine. In: Neidhardt, F.C., Ingraham, J.L., Schaechter, M., Brooks, K., Magasanik, B., Umbarger, H.E. (Eds.), *Escherichia coli* and *Salmonella typhimurium*: Cellular and Molecular Biology, vol. 1. American Society for Microbiology, Washington DC, pp. 244–284.
Roberts, J., 1997. Control of the supply line. Science 278, 2073–2074.
Senn, H., Lendenmann, U., Snozzi, M., Egli, T., 1994. The growth of *Escherichia coli* in glucose-limited chemostat cultures: A reexamination of the kinetics. Biochem. Biophys. Acta 1201, 424–436.
Shoemaker, J., Reeves, G.T., Gupta, S., Pilyugin, S.S., Egli, T., Narang, A., 2003. The dynamics of single-substrate continuous cultures: Role of transport enzymes. J. Theor. Biol. 222, 307–322.
Smith, R.W., Dean, A.C.R., 1972. β-galactosidase synthesis in *Klebsiella aerogenes* growing in continuous cultures. J. Gen. Microbiol. 72, 37–47.
Tempest, D.W., Hunter, J.R., 1965. Magnesium-limited growth of *Aerobacter aerogenes* in a chemostat. J. Gen. Microbiol. 39, 355–366.
Tempest, D.W., Herbert, D., Phipps, P.J., 1967. Studies on the growth of *Aerobacter aerogenes* at low dilution rates in a chemostat. In: Microbial Physiology and Continuous Culture. HMSO, London, HMSO, pp. 240–253.
Vogel, U., Jensen, F.F., 1994. The RNA chain elongation rate in *Escherichia coli* depends on the growth rate. J. Bacteriol. 176, 2807–2813.
Yagil, G., Yagil, E., 1971. On the relation between effector concentration and the rate of induced enzyme synthesis. Biochem. J. 11, 11–17.
Yun, H.S., Hong, J., Lim, H.C., 1996. Regulation of ribosome synthesis in *Escherichia coli*: Effects of temperature and dilution rate changes. Biotechnol. Bioeng. 52, 615–624.
Zhang, X., Dennis, P., Ehrenberg, M., Bremer, H., 2002. Kinetic properties of *rrn* promoters in *Escherichia coli*. Biochimie 84, 981–996.